European Commission

JRC TECHNICAL REPORTS

A survey of computational models for blast induced human injuries for security and defence applications

Solomos, G

Larcher, M

Valsamos, G

Karlos, V

Casadei, F

2020

This publication is a Technical report by the Joint Research Centre (JRC), the European Commission's science and knowledge service. It aims to provide evidence-based scientific support to the European policymaking process. The scientific output expressed does not imply a policy position of the European Commission. Neither the European Commission nor any person acting on behalf of the Commission is responsible for the use that might be made of this publication.

Contact information
Name: Martin Larcher
Address: Via E. Fermi 2749, Ispra (VA), Italy
Email: martin.larcher@ec.europa.eu
Tel.: +390332789563

EU Science Hub
https://ec.europa.eu/jrc

Contents

Abstract

Explosions and blast waves can cause human injuries due to both the interaction of the blast waves with the human tissues and the generated and propelled fragments that strike the body. Several models for the prediction of these injurious effects have been reviewed in this report. They have been selected from those most widely established and more suitable for implementation in finite element codes for risk assessment in large-scale numerical simulations. The models examined have been presented according to the established three categories of primary, secondary and tertiary injury mechanisms. They are probabilistic and their probit (or logistic) functions are presented and explained. Appropriate pressure-impulse and mass-velocity diagrams are drawn for blast waves and fragment injuries, respectively. Comparisons of injury criteria predictions are made, and some merits or shortcomings of the models are indicated. A workable model of munition fragmentation is also included. Thus the report provides the means for an efficient assessment of human injury risk in case of explosion events, which can effectively contribute to refining methods of protection in security and defence.

.

1 Introduction

The terrorist attacks in Oklahoma City (1996), New York (2001), Madrid (2004), Moscow (2004), London (2005), Brussels (2016) have shown the vulnerabilities of our soft targets and public spaces. These form part of our modern societal system and include transport systems with congregation areas, recreational areas, sports stadia, open-air gathering places, squares etc. All of them are characterised by the lack of specialized protection measures, their open architecture and their widely dispersed assets. The most frequent way to carry out attacks has been the use of explosive devices [1], which is also the most deadly compared to other modus operandi such as armed attack, sabotage, and arson. Bombs are relatively easy and cheap to construct, with detailed instructions on how to build various forms of explosives readily available online [2]. While intelligence and other security measures will always play the major role in preventing and foiling such attacks, improved architectural design may also significantly contribute towards mitigating the effects of explosions. Thus reliable simulation tools for assessing structural vulnerabilities and human injuries in case of an attack with explosives are indispensable.

The potential of an explosive device to inflict injury, via the generated blast wave and fragments, depends on many parameters like the size and composition of the explosives, the location of the human relative to the bomb, the medium in which the explosion takes place, the geometry of the surrounding area. For example, for people in close proximity to a wall it is intuitively expected that they will be subject to enhanced blast overpressure and be at a higher risk of blast injury. A blast wave in water propagates rapidly with a slow rate of dissipation, as water is non-compressible, and thus has a greater potential for injury than does an explosion in air. In an open space, a blast wave spreads circumferentially from its origin and quickly dissipates, whereas an air blast wave decays much slower inside a closed space such as a long tube-like train or metro tunnel. A comparison of the injuries from detonations in confined structures and in open-air is presented in [3], [4], where it is shown that the mortality rate in confined spaces is higher. This implies that both the response of the air medium inside the structure and the failure of the structure itself have to be considered for the determination of the risk in case of a blast. Concerning the extent of human casualties, the number of deaths and injuries of the 2004 terrorist attack in Madrid is reported in [5].

State-of-the-art reviews of blast-induced injuries, concerning interesting aspects on their biophysics and pathophysiology, can be found in [6], [7], [8] and [9]. As emphasised there, some of these injuries, such as blunt and penetrating traumas due to flying debris and body impact, are immediately observable, while others may be initially occult and have a delayed onset of manifestation. These latter injuries are caused by complex interactions of the blast wave with the body tissues, especially those containing air, and the proper management of such internal injuries may become a challenge to civilian medical personnel. These problems can easily be exacerbated in mass-casualty situations, as bombs can injure enough people to overwhelm the resources in many communities [10], [11], [12].

Intensive research was undertaken already in the 1960s in order to examine human lethality from exposure to blast waves. For this purpose extensive experimentation with animals was carried out, and the results were statistically analysed, calibrated, scaled and transferred to human injury. Pioneering in this direction has been the relevant work and the report by Bowen et. al. [13], which is widely known and used as the "Bowen curves", Figure 1.. A Bowen curve is the plot of a relationship between P_r and T that gives the same lethality, i.e. probability of death (or alternatively, the same probability of survival). P_r and T are, respectively, the peak reflected overpressure and the positive phase duration of an ideal blast wave (see Chapter 2 and Figure 2, where the symbol t_d is used instead of T for the positive phase duration). Lethality was defined upon the animal's death or survival within 24 hours following its blast exposure. In total 2097 experiments on 13 different animal species were performed using shock tube apparatuses for generating the long duration shock pulses and explosive charges for the short duration ones.

More recently, the research group led by Bass has gathered and elaborated even more data in order to update and improve the Bowen curves. These data were collected from more than 2550 experiments with large animals from 55 different experimental studies (also those of the Bowen's dataset), out of which 1129 were finally used in the analysis [14]. They represented both open field and reflected wave conditions, and blast waves of both short and long duration pulses [15]. Relevant lethality/survival curves have been produced.

At the same time, numerous experiments were performed, principally for military applications, for investigating the potential injury and soldier incapacitation due to explosively propelled fragments [16]. Attention was focused on skin penetration and perforation and according to the open source information the quantification of these effects was made using post-mortem human subjects (PMHS, cadavers) and animal skin. The parameters to be taken into account included the projectile geometry (sphere vs cylinder) and mass, the velocity required for skin perforation or penetration, the skin origin (animal vs PMHS), and the skin backing (isolated skin vs skin still attached to the muscle).

The overarching objective of all these studies has been the development of models capable of predicting the injurious effects of explosions, due to both blast waves and propelled fragments, in order to ultimately use them to refine methods of protection. Many such models have been proposed, of varying sophistication and reliability, mostly formulated in a probabilistic manner. A big number of them has been collected and reviewed in the current report. Appropriate curves are drawn, comparisons and comments are made, and some backing and explanatory material is also supplied.

Of the above models, preference has been given to those appearing to be more apt for blast risk assessments in large-scale numerical simulations and in particular readily implementable in finite element (FE) codes. This is the case of the explicit finite element code EUROPLEXUS [17], in which several of the examined models have already been successfully implemented and tested [18], [19], [20], [21].
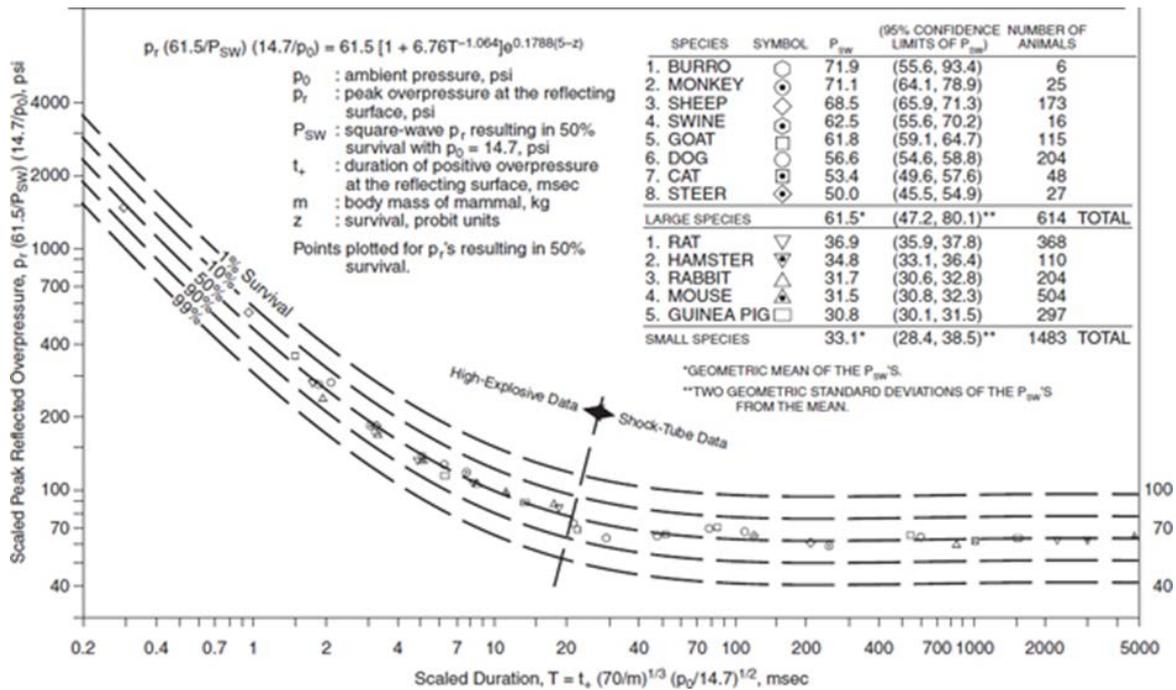
Figure 1. Survival curves (24-hour) applicable to sharp-rising blast waves, derived from the analysis of data of 12 mammalian species (excluding guinea pig). Source: Bowen et al., [13].

2 Explosives and explosion loads

Explosives are classified as high-order explosives (HE) or low-order explosives (LE) [22], [23], [24]. Examples of HE include TNT, C-4, Semtex, nitroglycerin, dynamite, and ammonium nitrate fuel oil (ANFO). Examples of LE include gunpowder, and most pure petroleum-based bombs, such as Molotov cocktails.

Air blast waves are herein considered to result from the detonation of a solid high-order explosive charge, which is expressed as a TNT equivalent [22], [25]. The magnitude of the overpressure of an air blast wave that arrives at a certain point depends on the distance, the type and the size of the charge. An idealised form of an overpressure-time function at a certain distance from the explosive is shown in Figure 2. The figure depicts an incident blast wave and a potential form of its reflection (in case it encounters a rigid surface). It must also be mentioned that a forced air flow (blast wind) is also generated, immediately following the overpressure. The pressure that the blast wind produces (dynamic pressure) may have to be taken into consideration in the risk analysis of blast effects.

Shown in Figure 2 are the main characteristics of a free-field air blast: the arrival time t_a (it includes the detonation time itself), the peak incident overpressure P_s above the reference pressure p_0 (atmospheric pressure, approximately equal to 10^5 Pa), the duration of the positive phase t_d, the minimum pressure, and the duration of the negative phase t_n. The positive impulse I is the integral of the overpressure curve over the positive phase. For this phase the total incident pressure P at time t can be adequately described by the modified Friedlander equation [16]:

$$P(t) = p_o + P_s(1 - \frac{t}{t_d})e^{-b\frac{t}{t_d}} \tag{1}$$

The time t is measured from the beginning of the positive phase, and b, is a constant influencing the decay of the overpressure curve.
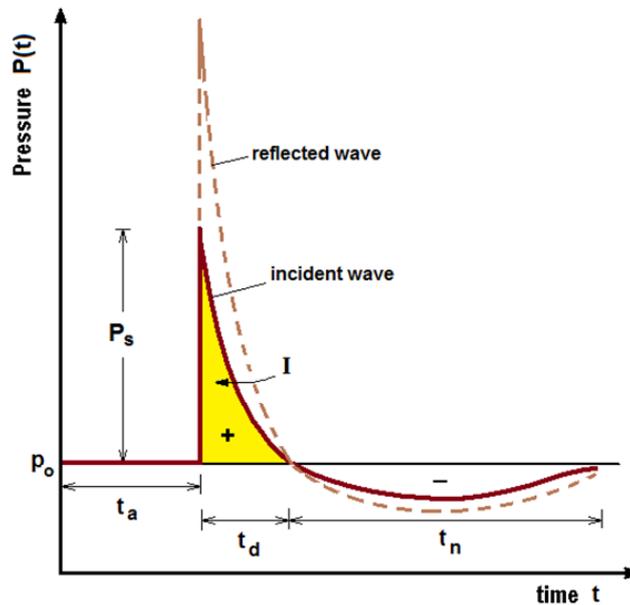
Figure 2. Idealised overpressure-time curve at a specific point from a high-explosive in free-field.

All parameters of eq.(1) can be readily found in appropriate diagrams and equations [26], [27], for free-field conditions both for spherical and hemispherical burst patterns. According to the Hopkinson-Cranz law, they are expressed through the dimensional scaled distance Z defined by eq.(2),

$$Z = \frac{R}{\sqrt[3]{W}} \tag{2}$$

5

where, R is the distance from the detonation source to the point of interest (m) and W is the mass of the explosive (kg).

Explosive and incendiary (fire) bombs are further characterized based on their manufacturing source [24]. "Manufactured" implies standard military-issued, mass produced, and quality-tested weapons. "Improvised" describes weapons produced in small quantities, or use of a device outside its intended purpose. Manufactured (military) explosive weapons are exclusively HE-based. However, terrorists will use whatever is available – illegally obtained manufactured weapons or improvised explosive devices (also known as "IEDs") that may be composed of HE, LE, or both and even homemade. Manufactured and improvised bombs may cause markedly different injuries [24].

3   Blast injuries

The modelling of injury and explosion effects considered below concerns mainly events in open spaces. Modifications to this modelling or a different approach should be followed when structural collapse or explosions inside confined spaces (buildings, large vehicles) are involved, which may change substantially morbidity and mortality. Traditionally, four basic mechanisms of blast injury are distinguished, which are termed as primary, secondary, tertiary, and quaternary [6], [7], [8] and [9]. The first three of them are pictorially shown in Figure 3.
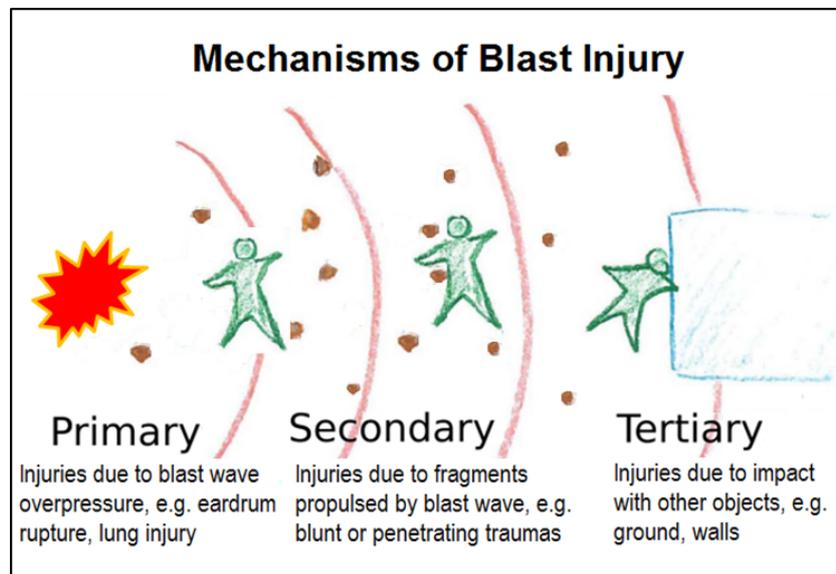
Figure 3. Schematic representation of blast injury mechanisms.

The primary mechanism refers to the interaction of the blast wave (overpressure) with the body and the transmission of the generated external force, due to large pressure differential, from the body surface to the internals. Acting for a few milliseconds, this force provokes rapid acceleration of the body wall and creates a relatively high-frequency stress wave, which propagates into the underlying tissues. Other proposed mechanical models for primary blast injuries also include concepts of spallation at water-gas interface, implosion of gas-containing structures with forceful re-expansion, acceleration and deceleration of organs relative to their fixation points and inertial effects on tissues of different densities. Particularly susceptible are air-containing organ systems, and specifically the lungs, the middle-ear and the bowel. Thus such injuries include blast lungs, eardrum (tympanic membrane) rupture, abdominal haemorrhage and perforation, globe eye rupture, concussion (Traumatic Brain Injury, TBI).

The secondary mechanism refers to injuries caused by fragments of the detonating device or by the generated flying debris, which are propelled by the blast wave and strike the human body. Blunt or penetrating traumas can be induced.

The tertiary mechanism refers to injuries due to the displacement of the whole body by the blast wind and its subsequent tumbling and sliding on rough surfaces, and its possible collision with hard obstacles (ground, walls etc.). Induced injuries include fracture and traumatic amputation, closed and open brain injury.

The quaternary mechanism refers to all injuries, illnesses, complications or disturbances due to exposure to explosions and not falling in the above three categories. They can appear in the form of burns, crush injuries, closed and open brain injury, asthma, pulmonary and other breathing problems from dust, smoke, or toxic fumes, angina, hypertension, post-traumatic stress disorder.

It is, of course, to be expected that blast injuries can be caused by the combination of more than one or all four of the above blast mechanisms. Polytrauma, i.e. injury involving multiple organs or organ systems, is the usual form of their manifestation.

4 Injury risk models

When studying explosion effects, the parameters calculated using references such as [26] comprise quantities like: arrival time, positive phase duration, peak incident overpressure, positive incident impulse, peak reflected overpressure, positive reflected impulse etc. Even when a more comprehensive finite element analysis is carried out, the standard output of the numerical simulation consists of the time histories of the pressure field in the air and the velocity of air particles and structural elements (if the structure is considered as deformable). The assessment of the human injuries risk at a point is not directly derivable from such data. There is need of an intermediate step relating values of the above calculated engineering quantities to the probability of occurrence of a specific type of human injury. It is, of course, understood that such an approach must be based on experimental biomechanical data with typical individuals (test animals or cadavers/PMHS) who have been subjected to well-specified blast loading or projectile shooting conditions.

4.1 PROBIT modelling

The probit function modelling takes account of the variation of the injury tolerance of a single, typical individual or in a population of similar individuals and connects probabilistically the "causative factor" (engineering quantities) with the "consequence" or "effect" (specific fatality or injury). The approach has been initiated in research with biological, agricultural and medical systems, as for example in what concerns the effectiveness of an insecticide with respect to the dosage applied [28], [29]. Specifically, when the causative factor of a specified intensity (dosage) is applied to the above population a certain proportion (e.g. 60%) of the exposed individuals suffers the specific effect (e.g. death, in case the mortality is examined) while the remaining (40%) are not affected at all. For another intensity of the causative factor this (death) proportion will be different, for a third intensity the (death) proportion will be again different, etc. It has been observed that when the logarithmic values of these intensities are plotted against the corresponding proportions, the resulting points follow an S-shaped curve, which is closely fitted by the cumulative distribution function (CDF) of a normal (Gaussian) distribution. This, of course, implies that the relationship between causative factor and (death) proportions must be of a lognormal distribution type.

The probit function is typically of the form [28], [29]:

$$Y = Y(S) = k_1 + k_2 \ln(S) \tag{3}$$

where, Y is the probit variable, k_1 and k_2 are constants, ln is the natural logarithm function (with base e), and S the "causative factor", an expression involving the engineering blast wave quantities (overpressures, impulses, velocities etc.). The constants k_1 and k_2 are determined in the above-mentioned fitting of the test data with the CDF of the normal distribution, and are adjusted so that the probit value of $Y=5$ corresponds to the death probability of 0.5=50%. Under this setting, the involved function is the shifted normal distribution with mean value equal to $\mu=5$ and standard deviation equal to $\sigma=1$. The corresponding PDF (probability density function) and CDF (cumulative distribution function), denoted as f(Y|5,1) and F(Y|5,1), respectively, are as follows

$$f(Y|5,1) = \frac{1}{\sqrt{2\pi}} e^{-\frac{(y-5)^2}{2}} \qquad F(Y|5,1) = \int_{-\infty}^{Y} f(y|5,1)dy \tag{4}$$

These functions are depicted in Figure 4. It must be noted that according to the f(Y|5,1) probability modelling, the values of Y should lie with probability 0.9973 in the interval $[\mu-3\sigma, \mu+3\sigma]=[2, 8]$, i.e. negative Y values should practically never be encountered.

### 4.1.1 Calculation of probability of injury or death

On the basis of the probit formulation, having evaluated the Y value, the fatality or injury probability $Pr(Y)$ is determined by simply evaluating the normal cumulative distribution function F(Y|5,1). Figure 4 shows schematically how from a Y value pertaining to a specific fatality (or specific injury) the probability of its occurrence is determined. Often instead of fatality or injury probability, the survival probability is used, which is defined as

$$Survival\ probability = 1 - Death(Injury)\ probability \tag{5}$$

In this example, it can be seen that if $Y=5.75$ then this death probability is 0.773, and consequently the probability of survival would be 0.227 (=1-0.773). This calculation can be readily done by using Tables, such as those provided in [29], or nowadays easily by directly computing the cumulative distribution function $F(Y|5,1)$:

$$\Pr(Y) = F(Y|5,1) = \int_{-\infty}^{Y} f(y|5,1)dy = \int_{-\infty}^{Y-5} \frac{1}{\sqrt{2\pi}} e^{-\frac{y^2}{2}} dy = \Phi(Y-5|0,1) \tag{6}$$

The symbol $Pr(.)$ stands for probability and $\Phi(.)$ is the CDF of the standardised normal distribution ($\mu=0$, $\sigma=1$ in eq.(4)), which is exhaustively tabulated in the mathematical literature.
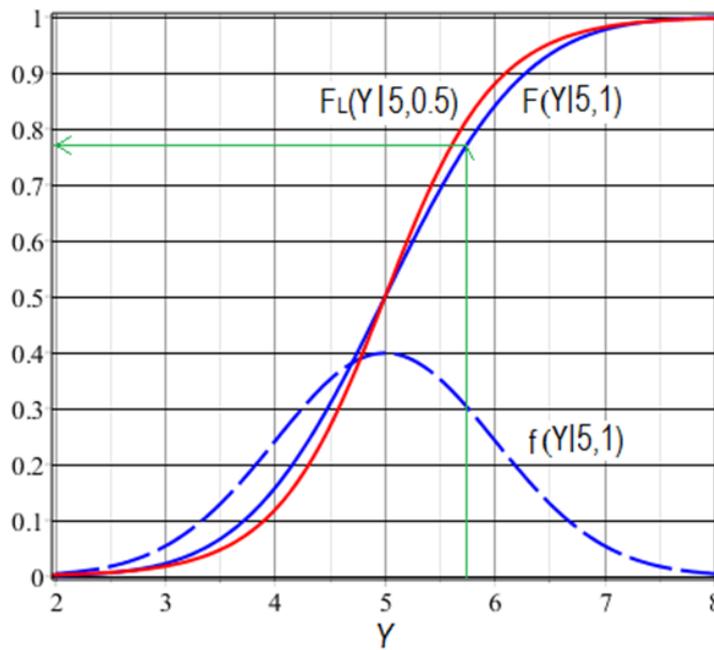

Figure 4. Normal probability density function f(Y|5,1), its corresponding cumulative distribution function F(Y|5,1) and the Logistic F_L(Y|5,0.5).

As an alternative to the above numerics [30], the probability of occurrence $Pr(Y)$ of a specific fatality or injury can be determined using the polynomial expression of eq.(7), which is an approximation to the above cumulative normal distribution F(Y|5,1),

$$\Pr{}^*(Y) = 0.01(-3.25Y^3 + 48.76Y^2 - 206.6Y + 270.35) \tag{7}$$

The functions $Pr(Y)$ and $Pr^*(Y)$ are compared in Figure 5. As clearly seen, the Pr^* approximation is very good in the Y interval [3.75, 6.25], it is acceptable also in the interval [2.8, 7.2], but it should not be used outside this latter interval.
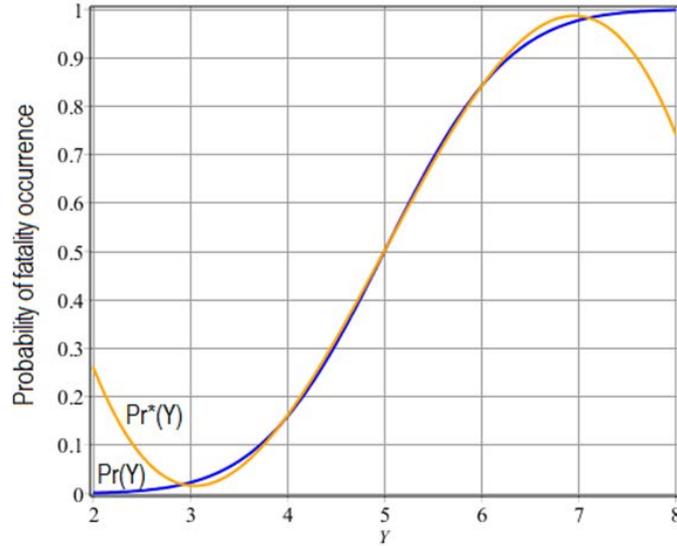
Figure 5. Probability of fatality (or injury) occurrence *Pr(Y)* and its polynomial approximation *Pr*(Y)*.

4.1.2   Pressure-Impulse diagrams

As shown above, the probability of fatality/injury occurrence *Pr(Y)* is readily calculated once the value of the appropriate probit *Y* has been determined. This may be a satisfactory end of the investigation, if assessing this probability is the result sought.

However, this is limitative since a single probability value does not provide any insight on the specific influence and possible interaction of the physical variables involved in order to arrive to this result. Also, a small variation in the values of the physical variables, would require another such (lengthy) calculation to be made. An efficient way of addressing this problem is the use of Pressure-Impulse (*P-I*) diagrams, whose construction is explained below [22].

As mentioned earlier, concerning human injuries the two main parameters of the impinging blast wave are its maximum overpressure (P_s) and impulse (*I*), Figure 2. Naturally, it is then the case that the causative factor *S* in eq.(3) is expressed in terms of P_s and *I*, and consequently the probit *Y* is a function of P_s and *I*, i.e. $Y=Y(P_s,I)$. Eq.(6) can then be written as

$$\Pr(P_s,I) = \Phi(Y(P_s,I)-5|0,1) = \frac{1}{2}\left(1+erf\left(\frac{Y(P_s,I)-5}{\sqrt{2}}\right)\right) \tag{8}$$

where the CDF of the standardised normal distribution *Φ(.)* has been expressed through the error function *erf(.)* [31].

The last equation indicates that the probability of fatality/injury can be expressed as a function of the two variables P_s and *I*. Further, if the value of this probability is fixed, say *Pr(.)=X1%*, then eq.(8) becomes

$$\frac{1}{2}\left(1+erf\left(\frac{Y(P_s,I)-5}{\sqrt{2}}\right)\right) = X1\% \tag{9}$$

and can be implicitly plotted for the variables P_s and *I*, producing a graph, which is schematically shown in Figure 6 (clearly the polynomial expression *Pr** of eq.(7) could be used in the left-hand side of eq.(9) in place of the function *Φ(.)*, recalling the relevant approximation constraints)
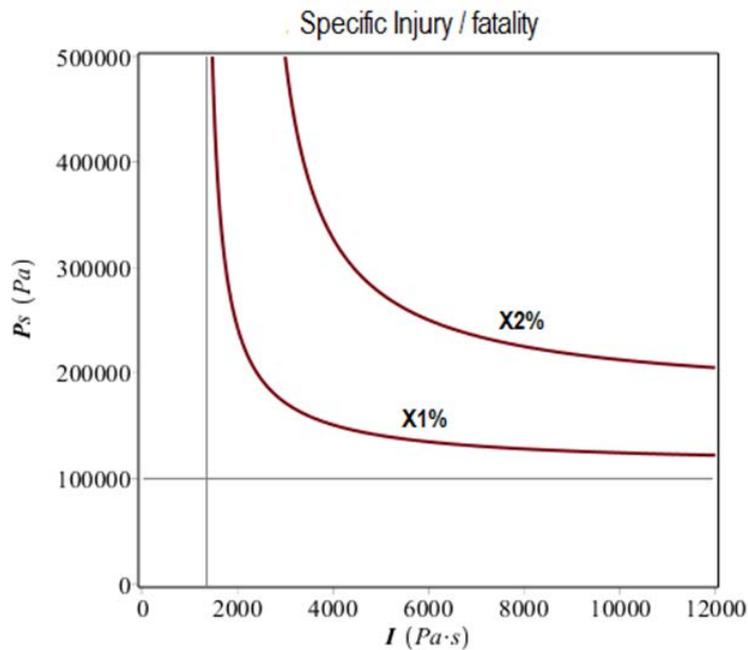
Figure 6. Example of Pressure-Impulse (P-I) diagram.

Such a diagram emphasizes that there are combinations of peak overpressures and impulses that produce the same probability regarding the occurrence of a specific injury/fatality. For this reason the curves of a P-I diagram can be considered as iso-injury / iso-fatality contours. Interpreting the P-I diagram for the current example, it can be seen that the curve *X1%* divides the (P_s,I) domain in two regions:

   i)   Pressure-impulse combinations found on this curve will cause with probability *X1%* the occurrence of the specific injury/fatality (Survival probability =100%-X1%);

   ii)   Combinations found to the right and above this curve will cause the occurrence of the specific injury/fatality with probability greater than *X1%*;

   iii)   Combinations falling to the left and below this curve will cause the occurrence of the specific injury/fatality with probability smaller than *X1%*,

If another probability value is chosen in eq.(9), for example *X2%>X1%*, another curve will be constructed in the (P_s,I) domain, lying to the right and above with respect to the X1% curve, etc.

The P-I diagram may also effectively demonstrate interesting trends of the iso-contours, which are characteristic of the underlying specific injury mechanisms. In Figure 6, for example, there appears to exist one horizontal asymptote at Ps≈100000Pa and a vertical asymptote at I≈1500Pa·s. This would mean that the specific injury/fatality will never occur (i) if the overpressure is below 100000Pa no matter how large the impulse is, or (ii) if the impulse is below 1500Pa·s no matter how large the overpressure is.

It is worth mentioning that often in literature instead of *P-I* diagrams one finds *P-t_d* diagrams, where t_d denotes the positive phase duration. These are equivalent representations because the positive impulse *I* is directly related to the peak overpressure and the positive phase duration, as clearly seen in Figure 2.

For some specific injuries/fatalities the formulation of the causative factor *S* of eq.(3) may not include the parameters of overpressure and impulse, and consequently a *P-I* diagram is meaningless. As will be seen below, for injuries due to blast propelled fragments/debris the causative factor is formulated in terms of the mass and the velocity of the striking fragments. In this case, it is convenient to construct a Velocity-Mass diagram, when the model allows to do so.

4.2 Other modelling approaches

For completeness it should be mentioned here that for the modelling of the variability of the human injury tolerance, the Logistic probability distribution is also widely employed [14], [32]. This distribution contains two parameters (m and s) and its CDF is given by eq.(10), where the variable Y represents the causative factor (expressed in a functional form of the engineering quantities, but not necessarily the same as in the Y equations above). Its CDF has a sigmoid form and for certain choices of the parameter values it can look very similar to the normal distribution, as shown in Figure 4, where it is plotted for $m=5$ and $s=0.5$.

$$F_L(Y|m,s) = \Pr(Y) = \frac{1}{1 + e^{-\frac{Y-m}{s}}}$$

(10)

Its advantage over the probit equations lies in the fact that it has an explicit mathematical expression, eq.(10), and thus the injury (death) probability is directly calculated without the use of mathematical tables etc. One such Logistic function will be presented in the following sections.

Finally, it is worth pointing out the parallelism of the probits for human injury with the approach followed for the assessment of damage to mechanical systems, e.g. buildings, whose resistance (capacity) is described with uncertainty, and are subjected to loadings which are also described with uncertainty (seismic loads). In this case S-shaped "fragility curves" are produced which describe the probability of "failure", conditioned on the load, over the full range of load values to which the system may be exposed. A structure is said to fail when it does not meet predefined limit state conditions. Thus, more than one fragility curves can be constructed, e.g. corresponding to states such as: "serviceable but impaired", "not serviceable", "collapsed" etc. In an analogous manner, more probits can be developed for the vulnerability of humans to explosion effects, e.g. corresponding to ear injuries, death due to lung haemorrhage etc. Also for the damage in mechanical systems, the lognormal distribution (with its subsequent transformation to the normal one) is naturally suitable for the modelling of the loading and/or the structural capacity [33].

5 Primary mechanism injuries

5.1 Death due to lung haemorrhage

Lethal lung damage should depend on both overpressure and impulse since it has been confirmed from the original work of Bowen et al. [13] and also [14], [15], [34] that different results are obtained for short- and long-duration blast waves. The body mass and orientation has also been found to play significant role, and an equation taking into account all these factors has initially been proposed in [13] and re-formulated in [23] and [35], [36]

$$Y = 5 - 5.74 \ln \left(\frac{4.2 p_o}{P_{eff}} + \frac{1.3}{I_{sc}} \right) \tag{11}$$

where P_{eff} is the effective pressure and I_{sc} is a scaled impulse, given by the expression

$$I_{sc} = I / (p_o^{1/2} m_p^{1/3}) \tag{12}$$

In these equations m_p= mass of person in kg; for a typical adult man weighing m_p=70kg eq.(11) becomes

$$Y = 5 - 5.74 \ln \left(\frac{4.2 p_o}{P_{eff}} + \frac{1694}{I} \right) \tag{13}$$

For individuals having substantially different body masses the last equation (and the following ones) will have to be re-calculated. The values suggested for m_p in in [23], [35] are: 5kg for babies, 25kg for small children, 55kg for women and 75kg for adult men.

The effective pressure depends on the orientation of the human body with respect to the propagating blast wave, and is calculated as follows (p_o=105 Pa is the atmospheric pressure):

i) For a person standing in the free field (the body long-axis is perpendicular to the direction of propagation of the blast wave), P_{eff} is the sum of the peak incident overpressure and the peak pressure from the high-velocity wind traveling directly behind the shock front, i.e.

$$P_{eff} = P_s + \frac{5 P_s^2}{2(P_s + 7 p_o)} = \frac{7 P_s (P_s + 2 p_o)}{2(P_s + 7 p_o)} \tag{14}$$

For the sake of demonstration, only for the current case the steps leading to the construction of the relevant *P-I* diagrams are outlined below. Eq.(14) is first substituted in eq.(13), and this in turn into eq.(8), which then becomes

$$\Pr(P_s, I) = \frac{1}{2} - \frac{1}{2} erf \left(4.0588 \ln \left(\frac{1.2 p_o (P_s + 7 p_o)}{P_s (P_s + 2 p_o)} + \frac{1694}{I} \right) \right) \tag{15}$$

Setting next specific probability values for $P_r(P_s,I)$ in eq.(15), e.g. $P_r(P_s,I)$= X1%= 0.75 ..., and plotting it implicitly over the variables P_s and I the *P-I* diagram of Figure 7 is obtained.

The last equation can also be plotted in 3D as a function of P_s and I, Figure 8. It is interesting to note that the curves of the *P-I* diagram can also be thought of as intersections of the three-dimensional surface of Figure 8 with planes parallel to the P_s and I axes.

An alternative form of *P-I* diagrams is also presented in Figure 9 and Figure 10. In particular, it has been chosen to show them in terms of "Survival probability" rather than "Death/Injury probability", the two quantities being connected through eq.(5).
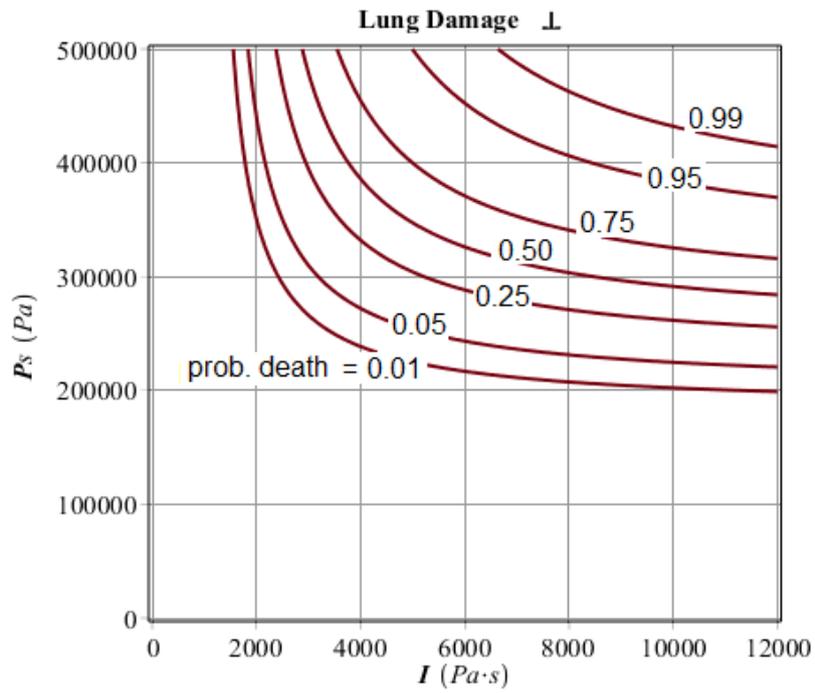
Figure 7. P-I diagram for the probability of death due to lung haemorrhage for a person standing in free field with the body long-axis perpendicular to the direction of propagation of the blast wave (person mass =70kg).
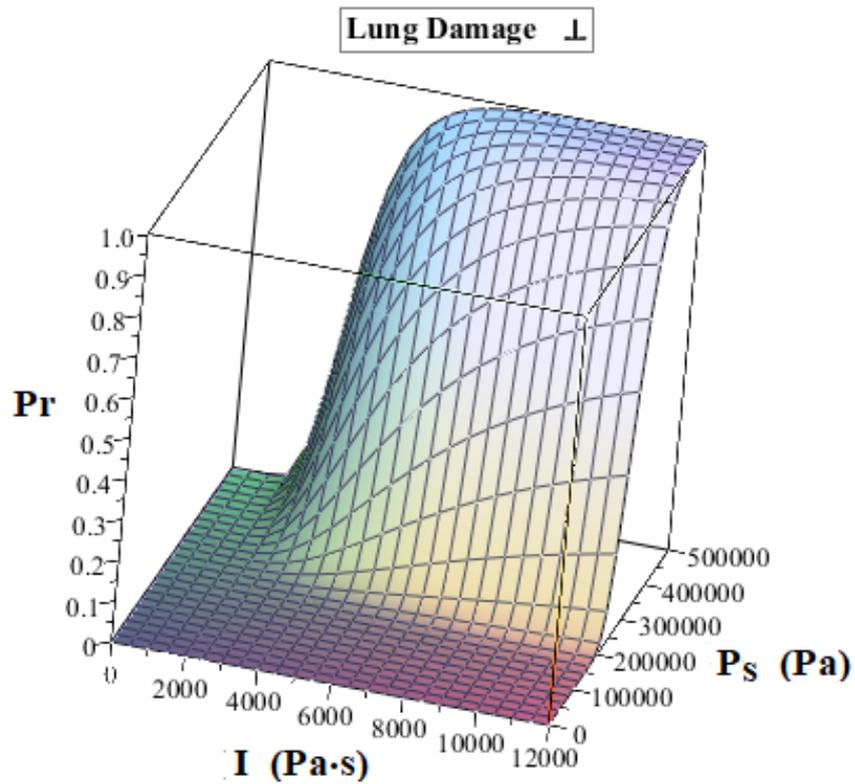

Figure 8. 3D plot of the probability of death due to lung haemorrhage for a person standing in free field with the body long-axis perpendicular to the direction of propagation of the blast wave (person mass =70kg).
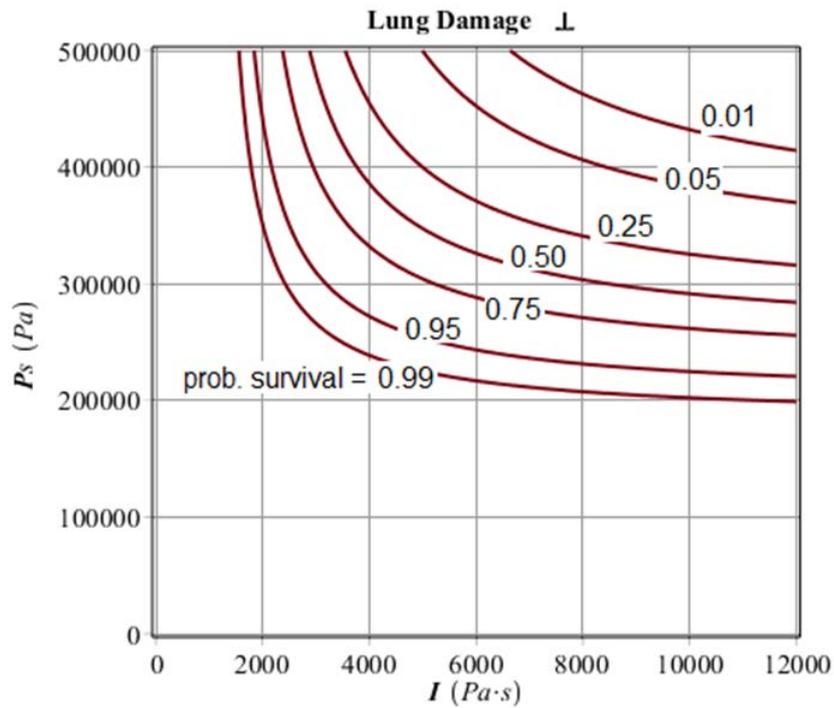
Figure 9. P-I diagram in terms of survival probability from lung haemorrhage for a person standing in free field with the body long-axis perpendicular to the direction of propagation of the blast wave (person mass =70kg).
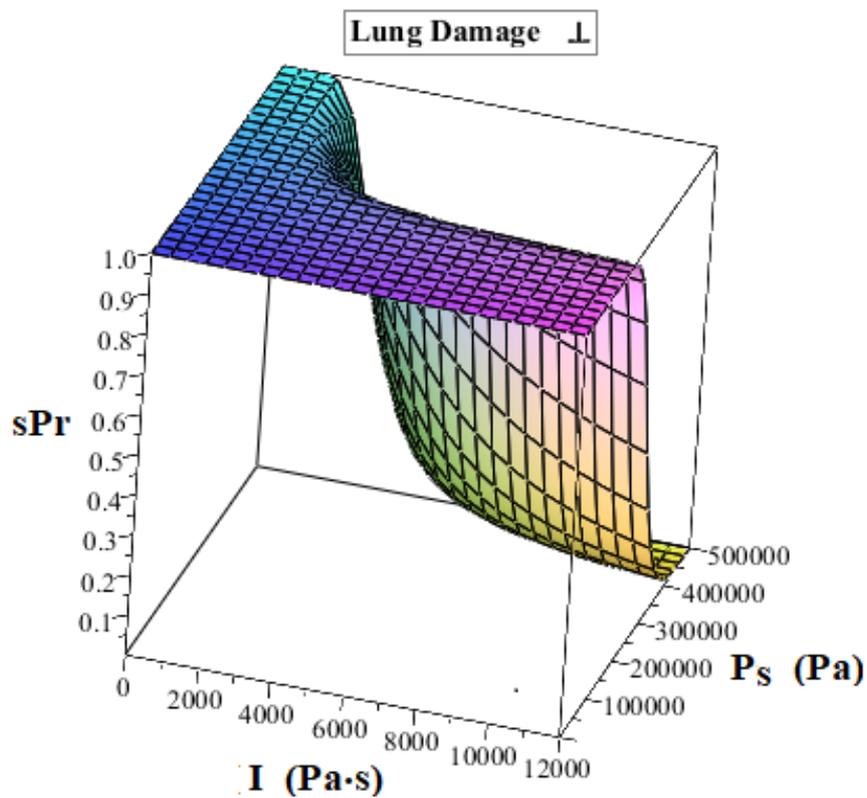
Figure 10. 3D plot of the survival probability from haemorrhage for a person standing in free field with the body long-axis perpendicular to the direction of propagation of the blast wave (person mass =70kg).

ii) For a person in prone or supine position, whose body long-axis is parallel to the direction of propagation of the blast wave, P_{eff} is equal to the peak incident overpressure, i.e.

$$P_{eff} = P_s \qquad (16)$$

The relevant *P-I* diagram is drawn in Figure 11.

iii) For a person standing or lying close to a reflecting surface (which is perpendicular to the direction of propagation of the blast wave), P_{eff} is the generated reflected pressure, which with a good approximation is given by the expression

$$P_{eff} = 2P_s \cdot \frac{4P_s + 7p_o}{P_s + 7p_o} \qquad (17)$$

Substituting in eq.(13) and using eq.(8), the relevant *P-I* diagram can be drawn, as shown in Figure 12.
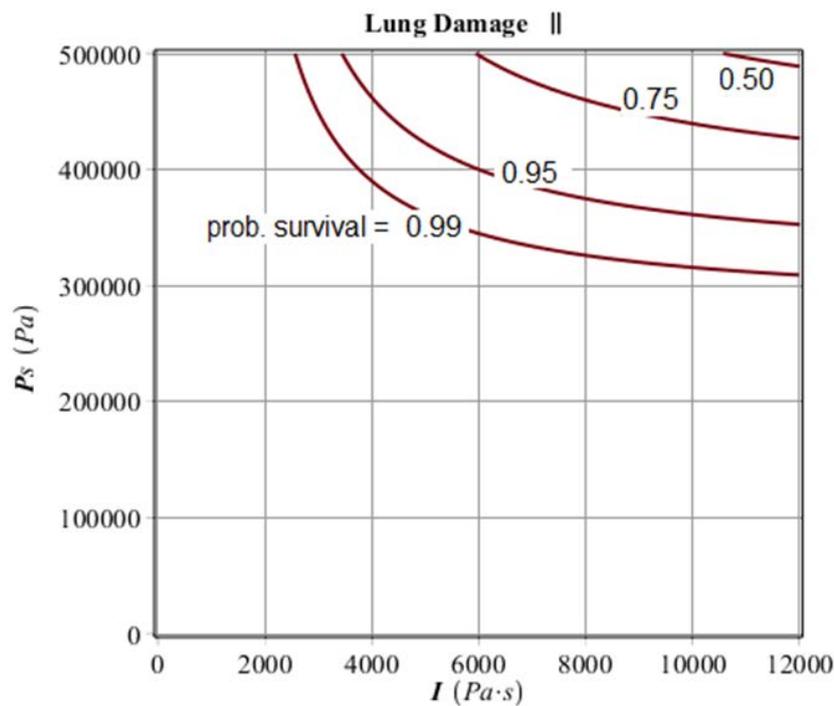
Figure 11. P-I diagram in terms of survival probability from lung haemorrhage for a person standing in free field with the body long-axis parallel to the direction of propagation of the blast wave (person mass =70kg).

NOTE: Attention should paid to the fact that for the above case i) "person standing in the free field with the body long-axis perpendicular to the direction of propagation of the blast wave", P_{eff} must include also the peak pressure from the blast wind. Thus, if blast pressures are determined with finite element techniques, for the case i) what is calculated is the incident pressure P_s, which should then be augmented according to eq.(14) before it is substituted in eq.(13). The problem does not exist for the cases ii) and iii) as the finite element calculations will automatically provide the correct P_{eff}.
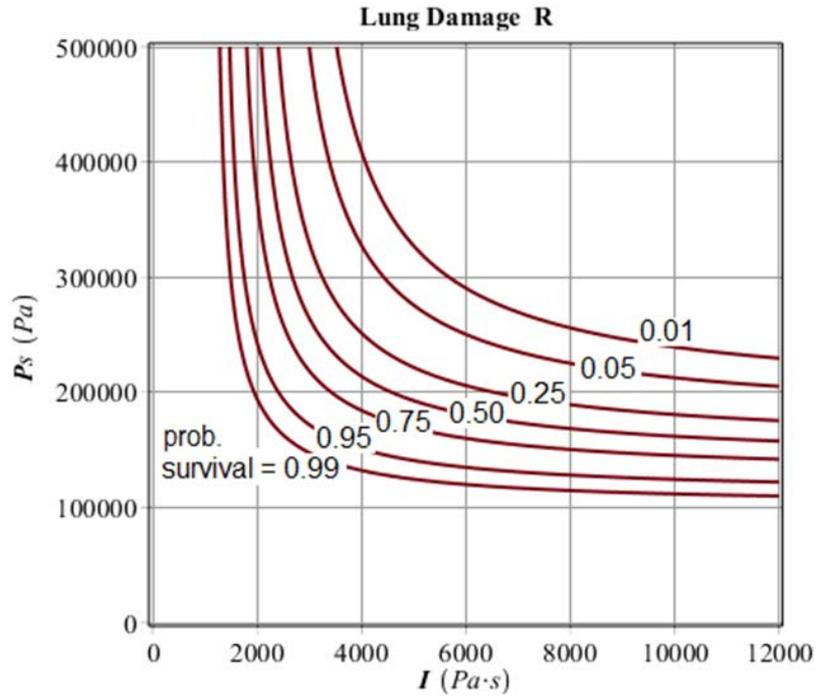
Figure 12. P-I diagram in terms of survival probability from lung haemorrhage for a person positioned close to a reflecting surface perpendicular to the direction of propagation of the blast wave (person mass =70kg).

5.2 Eardrum rupture

The biomechanics of this injury has been discussed in [37]. According to it, the ear is unable to respond faithfully to a pulse with a period of less than 0.3ms (even though it responds to sinusoidal sound waves in the frequency range 20-20000Hz), and attempting to do so results in a single, large excursion, which causes eardrum rupture. This behaviour is governed by the peak overpressure and its initial rise time (which for HE is practically zero).

The relevant probit equation of eardrum rupture, based on the data of [37], is described using the following expression [37], [35].

$$Y = -12.6 + 1.524 \ln(P_p) \tag{18}$$

where P_p is the peak incident or reflected overpressure, depending on the situation examined. Since the causative factor in the probit does not depend on the impulse I, the P-I diagram for eardrum rupture consists of lines parallel to the I-axis.
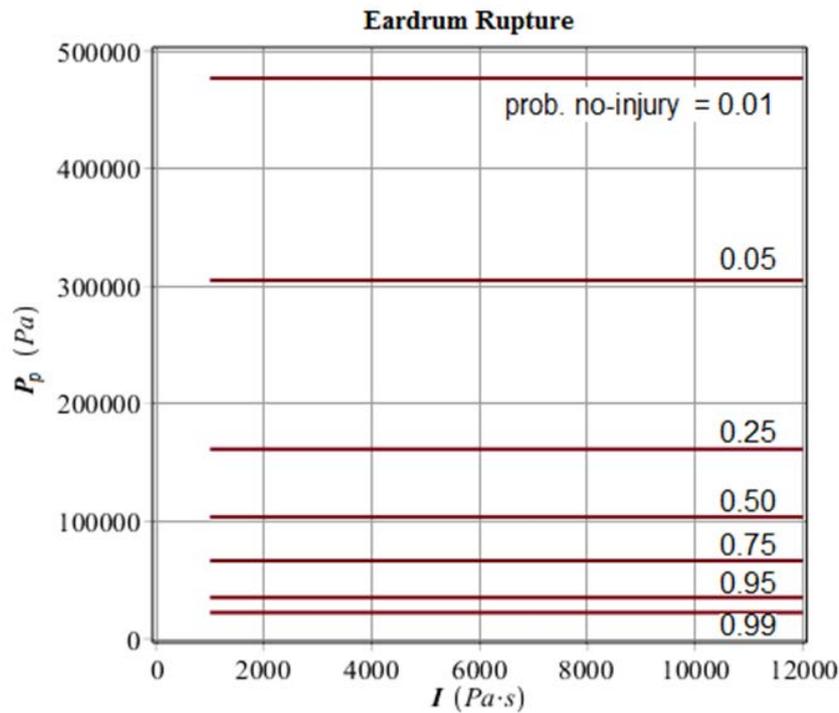
Figure 13. P-I diagram in terms of survival (no-injury) probability from eardrum rupture.

5.3 Case study

As an exercise on primary mechanism blast injuries, the probability curves are plotted in Figure 14 for the several cases of injury and death, keeping a constant value for the impulse I=3000 Pa·s and varying the peak incident overpressure. As is intuitively expected, it is observed that, with increasing peak incident overpressure P_s, the dangerousness for a person (adult male, 70kg mass), exposed to such a blast environment, would be graded as follows:

1. Firstly, it would suffer eardrum rupture, if the person is found in a reflected wave zone;

2. Secondly, it would suffer eardrum rupture, if the person is found in free field;

3. Thirdly, it would suffer lung damage (death), if the person is found in a reflected wave zone;

4. Fourthly, it would suffer lung damage (death), if the person is found in free field with the body long-axis perpendicular to the direction of propagation of the blast wave;

5. Lastly, it would suffer lung damage (death), if the person is found in free field with the body long-axis parallel to the direction of propagation of the blast wave.
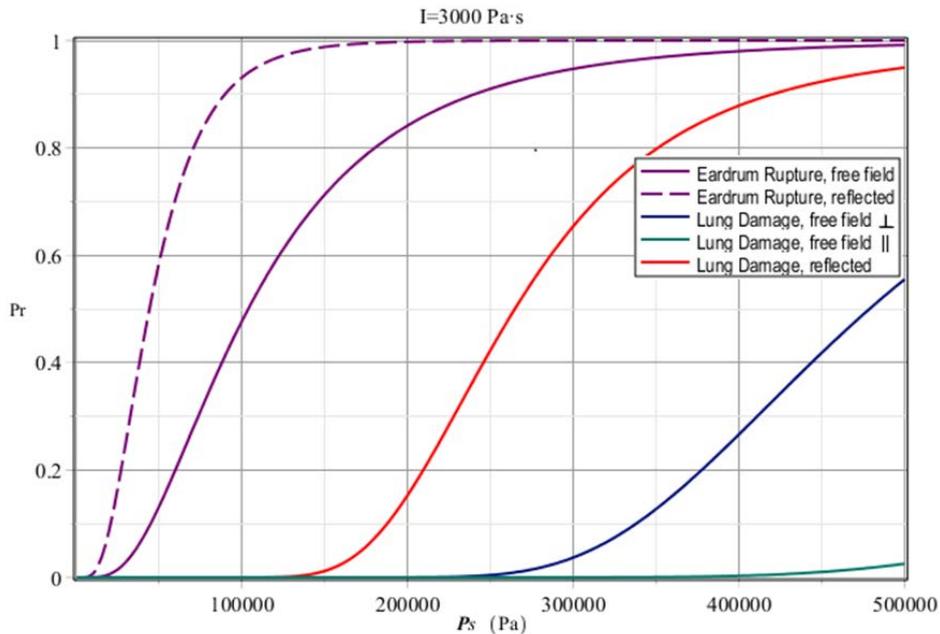
Figure 14. Probability of primary mechanism injury and death for constant impulse of I=3000 Pa·s and increasing peak incident overpressure P_s (person mass =70kg).

Figure 15 and Figure 16 are the same as Figure 14, with the difference that the value of impulse is kept constant at the level of I=6000 Pa·s and 12000 Pa·s, respectively. Some inversions in the previous dangerousness trend can now be noticed. The curves in Figure 15 show that for P_s greater than approximately 225000Pa (and I=6000 Pa·s), death for a person found in a reflected wave zone is more likely to come earlier than an eardrum rupture for the person in free field. It is also noticed in Figure 16 that such a trend inversion is encountered at approximately P_s=180000Pa for I=12000 Pa·s.

Clearly the position of the eardrum rupture curves does not change (it does not depend on impulse), and the order of dangerousness is as described before.
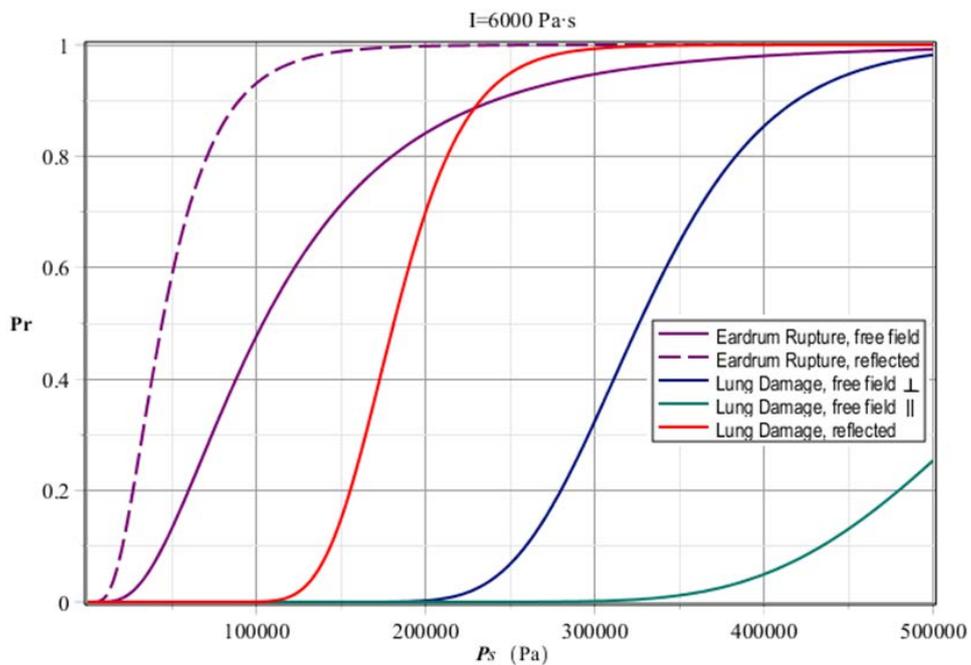
Figure 15. Probability of primary mechanism injury and death for constant impulse of I=6000 Pa·s and increasing peak incident overpressure P_s (person mass =70kg).
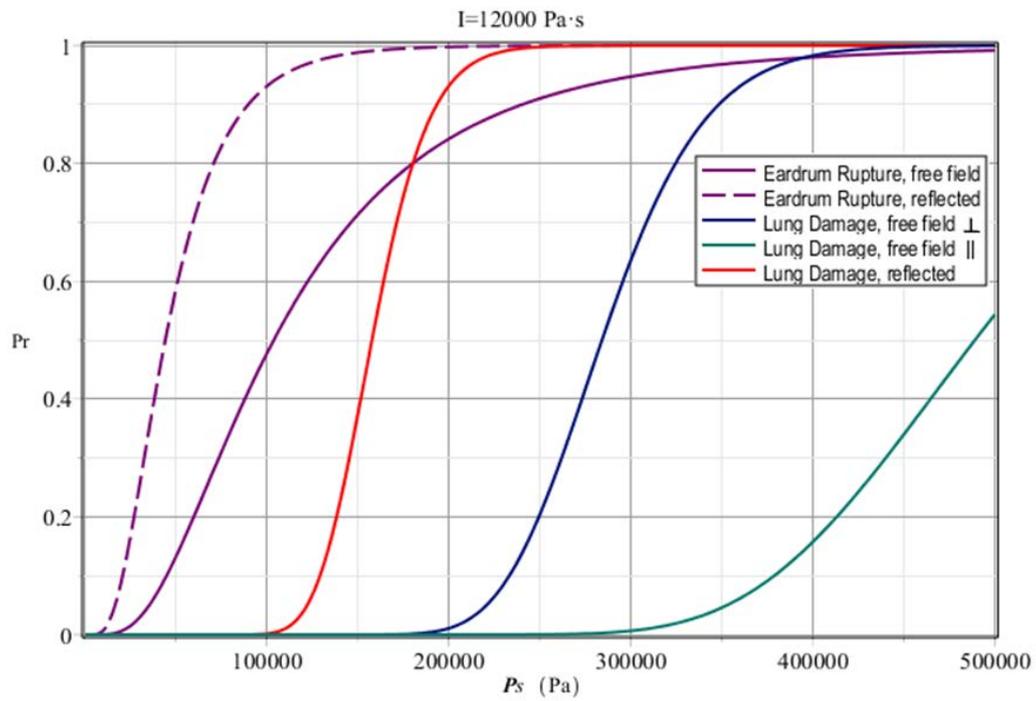
Figure 16. Probability of primary mechanism injury and death for constant impulse of I=12000 Pa·s and increasing peak incident overpressure P_s (person mass =70kg).

6   Secondary mechanism injuries

Secondary mechanism blast injuries are caused by fragments and/or flying debris impacting the human body. Research has shown that the kinetic energy of these particles, which involves their mass and velocity, along with their shape, are important parameters of their hazardousness with respect to their potential to cause blunt or penetrating traumas [32], [38]. It is customary to classify as (primary) fragments the accelerated particles resulting from the disintegrating detonation device, and as (secondary) debris those coming from fractured objects in the surrounding of the explosion, which are propelled by the blast wave.

6.1   The 80Joule-rule

A first quantification of this hazard dates back to 1906 when Rohne set the "80Joule-rule" [39], according to which a fragment is considered hazardous of incapacitation if it has at least 80 Joule of kinetic energy when it strikes the target person (the value of 78 Joules or 58 ft-lb is often reported). This simple criterion has been widely used and it still forms the basis of some security specifications, even though the interpretation of incapacitation has always been debated and criticized because it is not related to specific fatal and severe injuries [40].

6.2   The Lewis model

An improved empirical formula is used for the calculation of the risk due to the impact of fragments on the human body, which is based on the work of Lewis et al. [41], [42], [32], and involves skin full penetration as the injury criterion. The objective was to determine the probability of complete skin perforation since this occurrence is considered as a hazardous condition because the skin is more resistant to missiles than the underlying muscle. Therefore, if skin perforation occurs, the residual speed of the missile would be sufficient to cause a significant wound to organs or bones lying in the path of the missile. The investigations performed involved a variety of projectiles and striking velocities on a section of goat skin, which is not much different from human skin. A logistic model (not a probit) has been implemented and the resulting probability of skin perforation, as a function of the test variables, is of the form

$$P_{skin} = \frac{1}{1 + \exp\left[-\left(a + b\ln\left(\frac{m_f v^2}{10A}\right)\right)\right]} \tag{19}$$

P_{skin} is the probability of fatal injury (skin perforation), a and b are constants (Table 1.) determined after employing curve fitting techniques in the test results, m_f is the mass of the fragment in kg, v is its impacting velocity in m/s and A is the presented (or impact, or striking) area of the fragment in m^2 (exp(.) is the exponential function). As is intuitively expected, for skin penetration the causative factor is the term $m_f v^2/A$, i.e. the kinetic energy per fragment presented area. Attention is drawn to the fact that the units in the above equation are different from those in references [41] and [32], where m_f was expressed in grams, v in m/s and A in cm^2. As is easily observed, gram·(m/s)^2/cm^2 =10 [kg·(m/s)^2/m^2] =10 J/m^2, and for this reason, in order to not change the values for the parameters a and b, the factor 10 has been introduced in the denominator of the fraction in the above formula. Also, since a fragment is usually unstable and tumbling along its trajectory, the average presented area A_{av} can be used for the presented area A, which for any convex solid is equal to [43], [44], [45]

$$A_{av} = \frac{Total\ Surface\ Area}{4} \tag{20}$$

The Lewis criterion provides directly injury probabilities between 0 and 1. Figure 17 shows the relevant skin perforation probabilities for three conditions of skin coverage, where it is seen that special military uniforms offer additional protection. Ordinary clothing offers no such protection and it is on the safe side to consider the bare skin conditions in this case.

Table 1. Constants of the skin perforation Lewis formula.

Target	a	b
Bare skin	-28.42	2.94
Skin + 2-layer uniform	-48.47	4.62
Skin + 6-layer uniform	-50.63	4.51
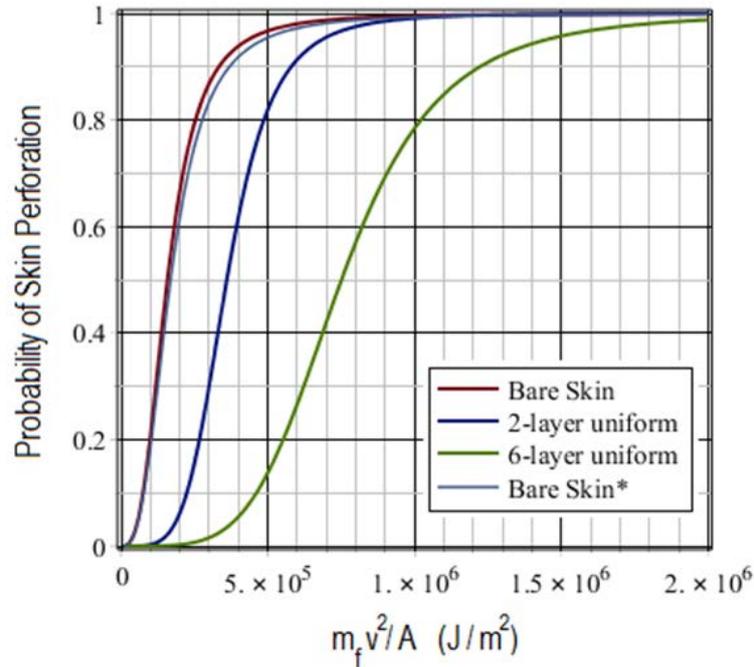
Figure 17. Skin perforation probabilities as functions of kinetic energy per fragment presented area (the curve "Bare Skin*" corresponds to slightly modified model constants, a=-27.35 and b=2.81).

The above logistic model has been derived from data with maximum projectile mass of less than 5g. The need for more data has always been pointed out, and other studies have been undertaken comprising experiments on animal or human skin either in-situ on cadavers (intact skin) or extracted (isolated skin) with projectile masses up to 15g. Different penetration resistance has been observed depending on the tautness of the skin sample, on the presence or not of the subcutaneous tissue, the shape of the fragment simulating projectiles etc. However, these datasets are not always homogeneous and of the same quality, and even the terms skin penetration and skin perforation have been used interchangeably without making the proper distinction [16].

6.3 The Gilbert probit equation

An analysis of this enriched dataset has been conducted in [46] and a probit equation for <u>bare skin</u> has been derived in the form

$$Y_1 = -17.0 + 1.535 \ln(\frac{m_f v^2}{A})$$
(21)

As above, in this equation m_f is the mass of the projectile in kg, v is its striking velocity in m/s and A is the presented area of the projectile in m^2.

Figure 18 shows the relevant skin perforation probabilities for this probit equation together with the previous curves of the logistic model. A huge difference is observed in the probability estimates of the two models for bare skin conditions. Surprisingly, the skin resistance to penetration according to the Y1-probit model appears to be several times greater than that of the logistic model for skin covered with the 2-layer uniform! It is suspected that there is some inconsistency in the data analysis or in the formulation of the above probit equation, especially in what concerns the units used. In fact, it is noticed that if the causative factor quantity $m_f v^2/A$ is multiplied by 10, the curves produced are definitely more comparable. Specifically, the above probit equation would be modified to

$$Y_2 = -17.0 + 1.535 \ln(10 \frac{m_f v^2}{A}) \tag{22}$$

with the units remaining as above. Skin perforation probabilities based on the Y2-probit are also plotted in Figure 18 (grey-color curve), where a plausible agreement is seen in the curves of the two models for bare skin conditions.
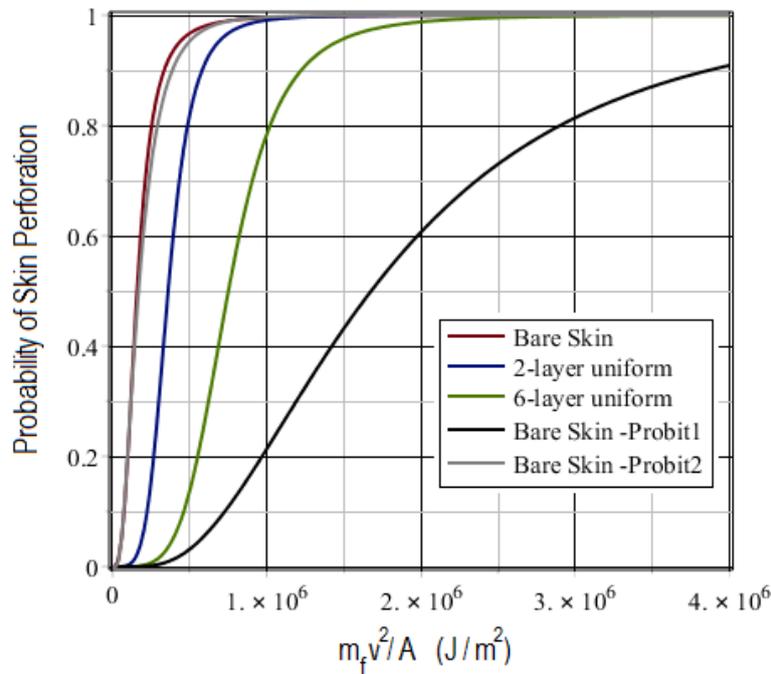
Figure 18. Comparison of skin perforation probabilities between the logistic model (three skin conditions) and the two probit models (for bare skin condition).

6.4 The V₅₀ equation

Another fatality criterion based on skin perforation has been developed in [42], [47], [48], it is applicable for bare skin conditions and is of the form

$$V_{50} = 1247.1 \frac{A}{m_f} + 22.03, \qquad \frac{A}{m_f} < 0.09; \ m_f \leq 0.015kg \tag{23}$$

also written as

$$V_{50} = 1247.1 \frac{1}{(k^2 m_f)^{1/3}} + 22.03, \qquad m_f \leq 0.015kg \tag{24}$$

V_{50} is the ballistic limit velocity, defined as the velocity (m/s) with 50% probability of skin perforation, and as above, A is the fragment presented area (m^2) and m_f the fragment mass (kg). The constant k is called the "shape factor" or "ballistic density" of the fragment/projectile and, expressed in terms of its mass and presented area, is equal to

$$k = \frac{m_f}{A^{3/2}} \tag{25}$$

Three models with their fragment velocity-mass diagrams for bare skin are compared in Figure 19 over their respective range of application. Clearly, only one curve can be drawn for the 80J-rule and the V_{50} equation, respectively, whereas several curves with different fatality probabilities can be produced with the Lewis model. It is observed that the V_{50} and the Lewis model curves are in good agreement at the 50% level fatality probability. It is also interesting to note that for smaller fragment masses (< 0.010kg) there is a region of velocities (associated to kinetic energy less than 80J), which according to the Lewis model imply almost certainly fatalities (probabilities >99%), while according to the 80J-model this region does not pose any risk of "incapacitation".
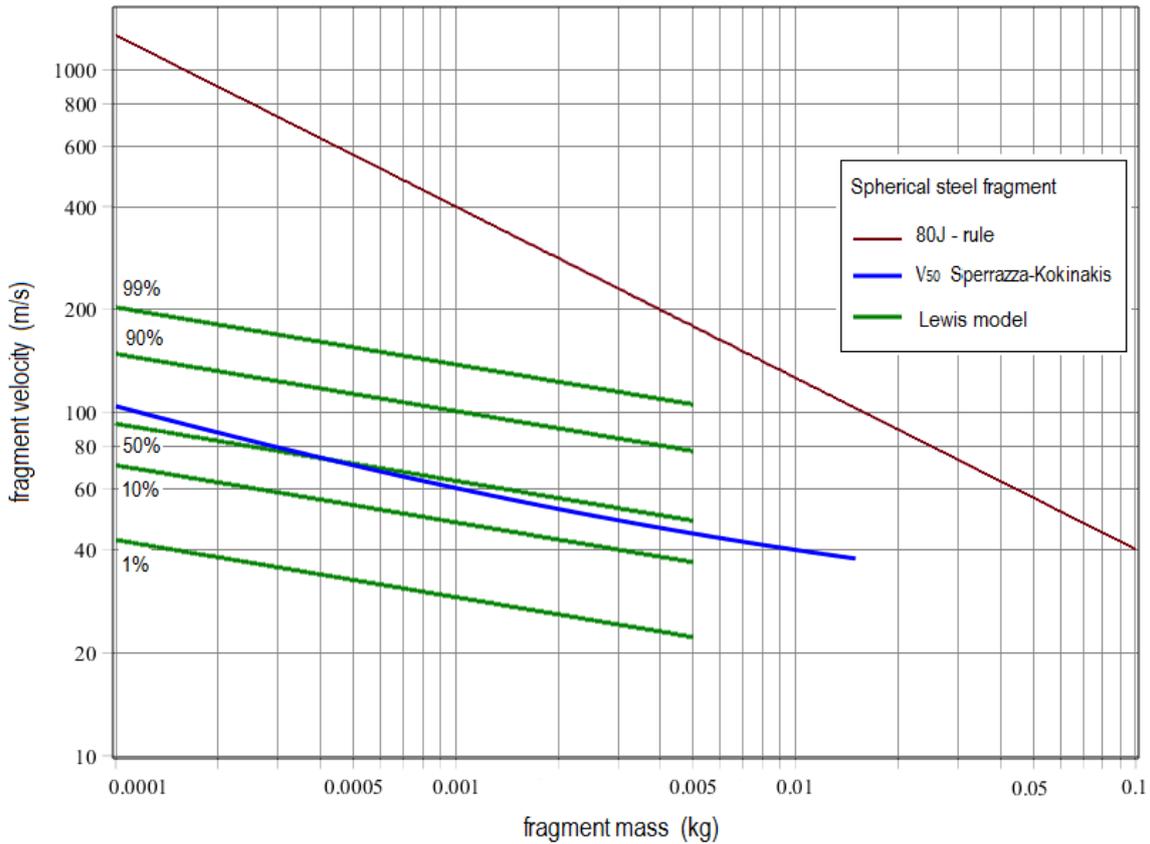
Figure 19. Velocity-mass diagrams for three fatality criteria based on skin perforation for bare skin conditions.

The curves plotted for V_{50} and the Lewis models refer to steel spherical fragments, for which it can be readily shown that: $m_f/A = [(16\rho^2)/(9\pi)]^{1/3} m_f^{1/3} = 325.3\, m_f^{1/3}$ (ρ= density of material = 7800 kg/m^3 for steel). For cubic fragments this quantity is equal to: $m_f/A = [(8\rho^2)/27]^{1/3} m_f^{1/3} = 262.2\, m_f^{1/3}$, where eq.(20) for the average presented area has been employed. The shape factor k would have, for steel spherical and cubic fragments, respectively, the values of 5867kg/m^3 and 4246kg/m^3.

6.5 The Greenbook formulae

Probit functions for death involving the velocity v and mass m_f of the fast moving fragments have also been developed in [35]. Three ranges of fragment mass values are distinguished, with their respective causative factor S, which reflects the corresponding principal mechanism and criterion of causing injury. They are as follows:

- for 0.001kg $\leq m_f \leq$ 0.1kg, where the fragment criterion is predominant

$$Y = -29.15 + 2.10\ln(m_f v^{5.115}) \tag{26}$$

- for 0.1kg $\leq m_f \leq$ 4.5kg, where the energy criterion governs

$$Y = -17.56 + 5.30\ln(\frac{1}{2}m_f v^2) \tag{27}$$

- for 4.5kg $\leq m_f$, where the probability of skull-base fracture is predominant

$$Y = -13.19 + 10.54\ln(v) \tag{28}$$

The units in the above expressions are kg for the mass and m/s for the velocity. It is noticed that the presented area of the fragment does not appear explicitly in the causative factor. The plot of this fatality criterion is presented in Figure 20. It is noticed that for the middle range of fragment masses (0.1kg $\leq m_f \leq$ 4.5kg) this criterion practically coincides with the 80J-rule and is overall more conservative. For comparison reasons, the curves of V_{50} for the models of Lewis and Sperrazza-Kokinakis have been drawn beyond their respective fragment mass application range.
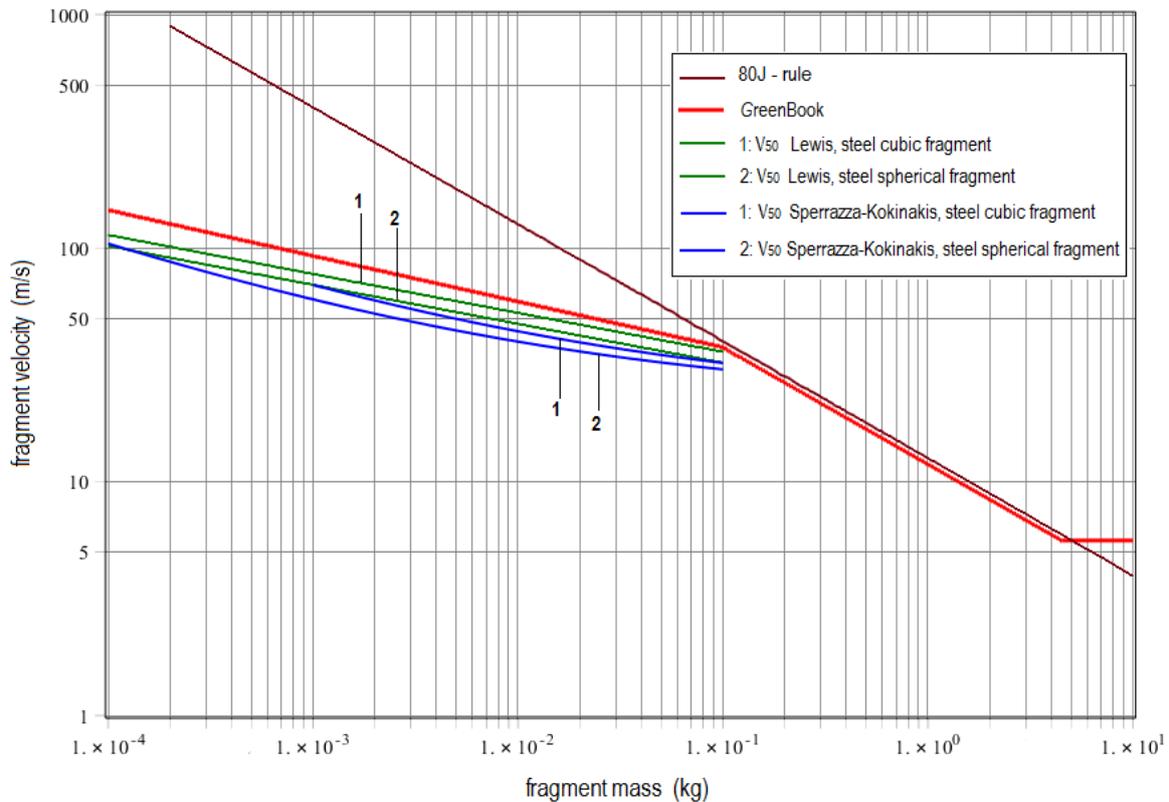
Figure 20. Velocity-mass diagrams for the GreenBook probits over a wide range of fragment masses and for three other fatality criteria for bare skin conditions.

6.6 Hit probability

The above criteria of human fatality/injury due to secondary blast mechanisms presuppose that a person is stricken by a fragment at first place. Therefore the above derived probabilities are not absolute, but conditional upon the event of the person being hit by a fragment following the explosion [38]. In the military terminology they are known as probabilities of "incapacitation" (I) given a hit (H), that is *Pr(I / H)*.

In simple situations and making several rough assumptions, the hit probability *Pr(H)* can be estimated at a specific stand-off distance R_{so}. For example, a simplistic scenario can include a) an explosion taking place at a flat ground level (hemispherical burst conditions), b) the angular distribution of launched fragments being uniform, c) in the vicinity of the detonation source the fragment trajectories being adequately approximated by straight lines. Assuming that the total number of fragments emitted is N and without considering their mass distribution, the hit probability for an exposed person at R_{so} can be calculated as follows.

The Poisson distribution is employed for modelling the number of hits that the person is subjected to [49]. The areal density *q* of fragments at a distance R_{so} is first defined as

$$q = \frac{N}{2\pi R_{so}^2} \tag{29}$$

which is the total number of fragments divided by the area of the hemisphere of radius R_{so} centred at the explosion source. The mean (average) hit rate λ is next calculated by multiplying *q* with the presented area S_b of the body of a person ($S_b \approx 0.58$ m^2),

$$\lambda = q S_b \tag{30}$$

According to the Poisson model, the probability of the number of hits to be *n* is equal to

$$\Pr[hits\,number = n] = \frac{e^{-\lambda}\lambda^n}{n!} \tag{31}$$

The probability of having zero hits (*n*=0) is $e^{-\lambda}$, and finally the hit probability, which implies at least one hit, is calculated as the difference of unity minus this latter probability:

$$\Pr[H] = \Pr[at\,least\,one\,hit] = 1 - \Pr[n=0\,hits] = 1 - e^{-\lambda} = 1 - \exp(-\frac{N}{2\pi R_{so}^2} S_b) \tag{32}$$

As a numerical application, the above derived formula is used for the simple case study with a person at R_{so}=15m and hit probability set at greater than or equal to 1%, i.e. Pr[H] $\geq$ 0.01. For this condition to be met it can be readily found that the number of fragments must satisfy $N \geq 24.5$, that is, the total number of fragments launched must be at least 25. Of course this does not yet say anything on whether (some of) these fragments will have the mass-velocity-geometry characteristics required to cause fatality according to the previously presented criteria.

Information on fragmentation, mainly referring to munition, and models for the fragment mass distribution and velocities are included in Annex A.

7 Tertiary mechanism injuries

Such injuries are due to whole body displacement and, as is intuitively understood, the inflicted injuries greatly depend on the maximum velocity imparted to the body due the blast effects. This velocity is usually assumed to be also the collision velocity with which the body subsequently strikes a rigid obstacle. **Error! Reference source not found.** and **Error! Reference source not found.** below provide some data of tests with animals concerning impact velocity and death probability for this injury type. The search of suitable probits entails the closest reproduction of such data by the models developed. As shown by the data of **Error! Reference source not found.** , impact of the skull (including the "coup-contrecoup" injury) is overall more critical than impact of the whole body. For example, lethality for skull fracture with 50% probability is expected at a velocity of 5.5m/s, whereas for whole body impact the same lethality level would occur at 16.5m/s.

Table 2. Data of tests with animals concerning impact velocity and death probability due to whole body displacement [50], [51], [36].

Skull fracture		Whole body impact	
Impact velocity (m/s)	Probability	Impact velocity (m/s)	Probability
3.0	Mostly "safe"	3.0	Mostly "safe"
4.0	Threshold	6.4	Lethality Threshold
5.5	50%	16.5	Lethality 50%
7.0	Near 100%	42.0	Lethality near 100%

Table 3. Data of tests with animals concerning dynamic pressure impulse, induced body velocity and death probability due to whole body displacement [52], [53].

| Dynamic pressure impulse (kPa·ms)	Peak horizontal body velocity (m/s)	Probability
8.78	0.092	No personnel blowdown
58.27	0.61	50% personnel blowdown
379.13	4.0	1% serious injury from being blown down (bone fracture…)

7.1 The Greenbook probit functions

One mechanical model employed in [35] for deriving the two probit functions below takes into account the force due to the dynamic pressure from the blast wind and calculates the velocity of the human body (upright, stiff-legged position), which is assumed to be of cylindrical shape, with a mass of 70kg and a presented area of 0.382m^2. This velocity is next correlated to the incident overpressure and impulse. As is recommended, the applicability of both probits is limited to P_s values lower than $4x10^5$ to $5x10^5$ Pa.

i) Death due to head impact on a hard surface and consequent <u>skull fracture</u> due to whole body displacement. Eq.(33) describes the probit function (Y_1), provided in [35], [36],

$$Y_1 = 5 - 8.49 \ln\left(\frac{2.43 \times 10^3}{P_s} + \frac{4 \times 10^8}{P_s \cdot I}\right), \qquad P_s < 5 \times 10^5 \tag{33}$$
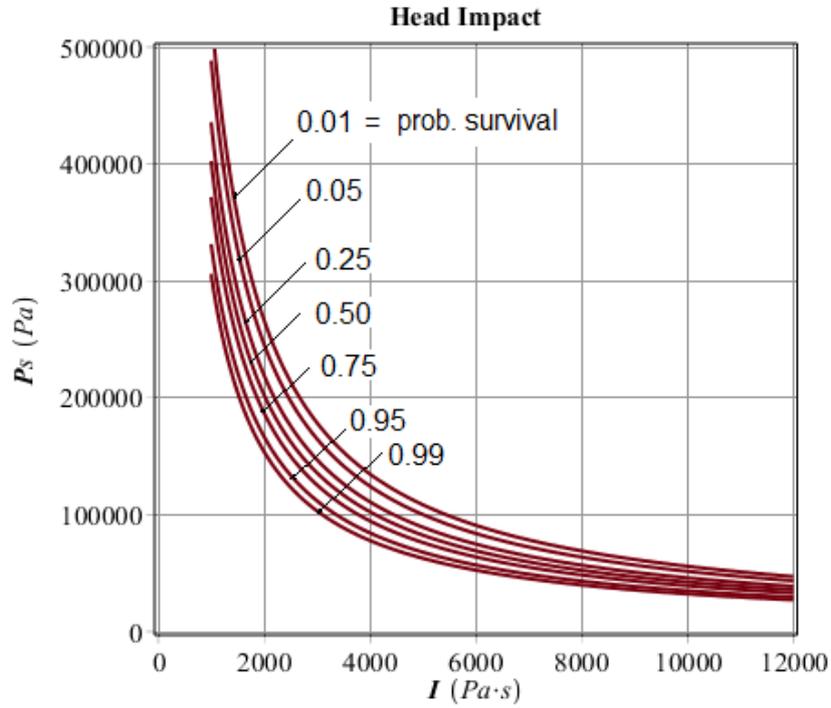
Head Impact

Figure 21. P-I diagram in terms of survival probability from head impact and rupture due to body displacement.
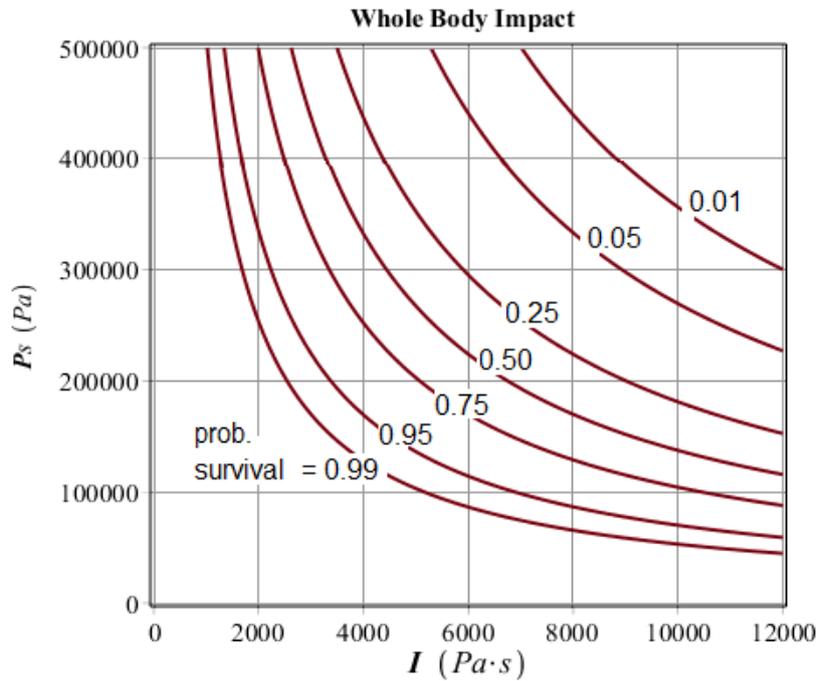
Whole Body Impact

Figure 22. P-I diagram in terms of survival probability from whole body displacement and impact on a hard surface.

ii) Death due to whole body impact (no specific part of the body is considered) on a hard surface due to whole body displacement. Eq.(**Error! Reference source not found.**) describes the probit function (Y_2), provided in [35], [36]

$$Y_2 = 5 - 2.44 \ln\left(\frac{7.38 \times 10^3}{P_s} + \frac{1.3 \cdot 10^9}{P_s \cdot I}\right), \qquad P_s < 5 \times 10^5 \tag{34}$$

Figure 21 and Figure 22 show the corresponding P-I diagrams, where it can be clearly seen that impact of the skull is more critical than impact of the whole body.

7.2 Additional models

Other researchers have carried out more elaborate investigations, considering both the overpressure and the dynamic wind pressure acting on the human body, and have formulated probits in terms of the maximum induced velocity. For lethality from <u>skull fracture</u> due to whole body displacement, using experimental data different from those in **Error! Reference source not found.** and **Error! Reference source not found.**, the following probit is provided in [54]

$$Y = -6.04 + 7.11 \ln(V_b) \tag{35}$$

where V_b is the body velocity (m/s).

Also, another probit can be found in [55] for lethality from <u>whole body impact</u> on hard surface due to whole body displacement, in the form

$$Y = -2.14 + 2.54 \ln(V_b) \tag{36}$$

The last two probits produce estimates that are in line with the data of **Error! Reference source not found.**. Specifically, it is observed that lethality with 50% probability (i.e. when Y=5) for skull fracture is obtained at velocity of 4.73m/s, and for whole body impact at 16.63m/s, respectively. For lethality with more than 99% probability (i.e. when Y=8) the corresponding velocities are 7.20m/s and 54.17m/s, respectively. The two probits are also consistent in the sense that they show that impact of the skull is more critical than impact of the whole body. The determination of the induced body velocity due to the blast effects remains always a non-trivial task.

8 Conclusions

Human injuries have been treated herein, which are due to both the interaction of the blast waves with the human tissues and the explosion generated propelled fragments that strike the body. A multitude of models for the prediction of these injurious effects have been proposed over the last decades and several of them have been selected and reviewed in this report. Preference has been given to those most widely established in the scientific community and at the same time appearing to be more apt for blast risk assessments in large-scale numerical simulations, and in particular readily implementable in finite element (FE) codes.

The models examined have been classified according to the established three categories of primary, secondary and tertiary mechanism injuries. They have a probabilistic formulation, and they consider lethality, i.e. probability of death, or alternatively probability of survival (the only non-lethal injury is eardrum rupture). Their probit (or logistic) functions are presented and all their parameters explained. Appropriate pressure-impulse and mass-velocity diagrams have been drawn for blast waves and fragment injuries, respectively. Comparisons of injury criteria predictions are made, and some supporting, explanatory material is supplied, too. Merits or shortcomings of the models have been indicated. An entire section in the Annex has also been dedicated to presenting a workable model of munition fragmentation.

The models presented can form a consistent framework for blast injury risk analyses. It must, of course, be underlined that these models have their limitations [56]. For example, in a strict sense they are applicable to a free field blast wave (Friedlander type) and not to complex blast waves which develop in situations of wave reflections, channelling etc. Also, the models only consider lethality (probability of death) and not degrees of injury. To overcome such limitations several other models have been developed, with varying degrees of sophistication and success. Among them, the following could be mentioned:

  i)   the Axelsson Blast Test Device (BTD) model for describing the chest wall response [57], which requires pressure input data from four transducers, and produces a measure of the degree of injury through the Adjusted Severity of Injury Index (ASII);

 ii)   the Weathervane SP model [58] that tries to simplify the Axelsson requirement by using only a single point (SP) field pressure to derive the ASII estimates;

iii)   the TNO approximation procedure to the Axelsson BTD model [59], which can accommodate complex blast pulses with multiple peaks.

Nevertheless, it is believed that the current collection of models with their documentation should still be of significant help when assessing the risk of human injury in case of explosion events. Identifying dangerousness and vulnerabilities can effectively contribute to refining methods of protection.

References

[1] National Consortium for the Study of Terrorism and Responses to Terrorism (START). Global terrorism database. Retrieved from http://www.start.umd.edu/gtd, 2012.

[2] Weimann, G. (2004). www.terror.net How Modern Terrorism Uses the Internet, United States Institute of Peace. Special Report 116.

[3] Leibovici D, Gofrit ON, Stein M, Shapira SC, Noga Y, Heruti RJ, Shemer J. Blast injuries: Bus versus open-air bombings – A comparative study of injuries in survivors of open-air versus confined space explosions. Journal of Trauma 1996; 41(6):1030–1035.

[4] Larcher, M, Casadei, F, Solomos, G. Influence of venting areas on the air blast pressure inside tubular structures like railway carriages, Journal of Hazardous Materials 2010; 183 (1-3): 839–846.

[5] Turégano-Fuentes F, Pérez-Diaz D, Sanz- Sánchez M et al. Overall Assessment of the Response to Terrorist Bombings in Trains, Madrid, 11 March 2004. Eur J Trauma Emerg Surg 2008; 34:433-441

[6] Wightman JM, Gladish SL, Explosions and blast injuries. Ann Emerg Med. June 2001; 37: 664-678.

[7] Horrocks CL, Blast Injuries: Biophysics, Pathophysiology and Management Principles, J R Army Med Corps 2001; 147: 28-40.

[8] Wolf SJ, Bebarta VS, Bonnett .J et al. Blast injuries. Lancet 2009; 374: 405-415.

[9] "3 Pathophysiology of Blast Injury and Overview of Experimental Data." Institute of Medicine. 2014. Gulf War and Health: Volume 9: Long-Term Effects of Blast Exposures. Washington, DC: The National Academies Press. doi: 10.17226/18253

[10] Frykberg ER, Medical management of disasters and mass casualties from terrorist bombing: how can we cope? J Trauma 2002; 53: 201-212.

[11] Almogy G, Belzberg H, Mintz Y, et al. Suicide bombing attacks: update and modifications to the protocol. Ann Surg. 2004; 239:295–303.

[12] Almogy G, Mintz Y, Zamir G, et al. Suicide bombing attacks: can external signs predict internal injuries? Ann Surg. 2006; 243:541–546.

[13] Bowen IG, Fletcher ER, Richmond DR, Estimate of Man's Tolerance to the Direct Effects of Air Blast, Technical Progress Report, DASA-2113, Defense Atomic Support Agency, Department of Defense, Washington, DC, October 1968.

[14] Bass CR, Rafaels KA, Salzar RS, Pulmonary injury risk assessment for short-duration blasts, Journal of Trauma, 2008; 65(3):604-615.

[15] Rafaels KA, Bass CR, Panzer MB, Salzar RS, Pulmonary Injury Risk Assessment for Long-Duration Blasts: A Meta-Analysis, Journal of Trauma, 2010; 69(2): 368-374.

[16] Breeze J, Clasper JC, Determining the velocity required for skin perforation by fragment simulating projectiles: a systematic review, J R Army Med Corps 2013; 159:265–270.

[17] http://www-epx.cea.fr/

[18] Giannopoulos G, Larcher M, Casadei F, Solomos G. Risk assessment of the fatality due to explosion in land mass transport infrastructure by fast transient dynamic analysis, Journal of Hazardous Materials 2010; 173:401–408.

[19] Larcher M, Casadei F, Giannopoulos G, Solomos, G, Planchet JL, Rochefrette A. Determination of the Risk due to Explosions in Railway Systems Proceedings of the Institution of Mechanical Engineers, Part F, Journal of Rail and Rapid Transit 2011; 225(4): 373-382.

[20] Larcher M, Forsberg R, Björnstig U, Holgersson A, Solomos G, Effectiveness of finite-element modelling of damage and injuries for explosions inside trains, Journal of Transportation Safety & Security, 2016; 8(S1): 83-100,

[21] Valsamos G, Casadei F, Solomos G, Larcher M, Risk assessment of blast events in a transport infrastructure by fluid-structure interaction analysis, Safety Science, 2019; 118: 887-897,

[22] Baker WE, Explosions in the Air, University of Texas Press, Austin and London, 1973.

[23] Baker WE, Cox PA, Westine PS, Kulesz JJ, Strehlow RA, Explosion Hazards and Evaluation, Elsevier, Amsterdam, 1983.

[24] Centers for Disease Control and Prevention CDC, Explosions and Blast Injuries: A Primer for Clinicians, U.S. Department of Health and Human Services, 2003.

[25] Karlos V, Solomos G, Calculation of Blast Loads for Application to Structural Components, Technical Report JRC87200, 2013.

[26] Kingery CN, Bulmash G, Airblast parameters from TNT spherical air burst and hemispherical surface burst, Tech. Rep., Defence Technical Information Center, Ballistic Research Laboratory, Aberdeen Proving Ground, Maryland, 1984.

[27] Karlos V, Solomos G, Larcher M, Analysis of the blast wave decay coefficient using the Kingery-Bulmash data. Int. J. of Protective Structures 2016; 7(3): 409-429.

[28] Fisher RA., Yates F, Statistical Tables for Biological, Agricultural and Medical Research. 6th Edition, Oliver & Boyd, Edinburgh and London 1963.

[29] Finney DJ, Probit Analysis. 3rd Edition, Cambridge University Press 1971.

[30] Ferradàs EG, Alonso FD, Doval Miñarro M, Miñana Aznar A, Gimero JR, Sanchez Perez JF, Consequence analysis by means of characteristic curves to determine the damage to humans from bursting spherical vessels, Process Safety & Environment Protection 2008; 86(2):121-129.

[31] Abramowitz M, Stegun IA, Handbook of mathematical functions with formulas, graphs, and mathematical tables, 9th Printing, Dover Publications 1970.

[32] Neades DN, Rudolph RR, An Examination of Injury Criteria for Potential Application to Explosive Safety Studies, component part AD-P004 883 of compilation report AD-A152 150: Minutes of the explosives Safety Seminar (21st), Houston Texas, 28-30 August 1984. Volume 2.

[33] Ellingwood BR, Structural reliability and performance-based engineering. Structures and Buildings 2008; 161(SB4):199–207.

[34] Cooper GJ, Taylor DE. Biophysics of Impact Injury to the Chest and Abdomen. J R Army Med Corps, 1989; 135: 58-67.

[35] Committee for the Prevention of Disasters, Green Book (1992), Methods for the Determination of Possible Damage to People and Objects Resulting from Releases of Hazardous Materials (1st Edition), CPR 16E, Directorate-General of Labour of the Ministry of Social Affairs and Employment, The Hague.

[36] Mannan S, Lees's loss prevention in process industries, Vol. 2, Hazard identification, Assessment and control, Elsevier, Amsterdam, 2005.

[37] Hirsch FG, Effects of overpressure on the ear – a review, Annals of the New York Academy of Sciences, 1968; 152(1): 147-162.

[38] Neades DN, Prather .N, The Modeling and Application of Small Arms Wound Ballistics, BRL-MR-3929, August 1991, U.S. Army Ballistic Research Laboratory, Aberdeen Proving Ground, MD.

[39] Rohne H, Schießlehre für Infanterie, 1906.

[40] SIPRI (Stockholm International Peace Research Institute), Anti-personnel Weapons, Lumsden M, Publisher: Taylor & Francis, ISBN 0-85066-128-5, 299pp., 1978.

[41] Lewis JH, Coon PA, Clare VR, Sturdivan LM, An Empirical/Mathematical Model to Estimate the Probability of Skin Penetration by Various Projectiles, Technical Report ARCSL-TR-78004, April 1978, US Army Armament Research & Development Command, Chemical System Laboratory, Aberdeen Proving Ground, MD.

[42] Sperrazza J, Kokinakis W, Ballistic Limits of Tissue and Clothing, BRL-TN-1645, January 1967, U.S. Army Ballistic Research Laboratory, Aberdeen Proving Ground, MD.

[43] Kokinakis, W, Sperrazza J, Criteria for Incapacitating Soldiers with Fragments and Flechettes, BRL 1269, January 1965, U.S. Army Ballistic Research Laboratory, Aberdeen Proving Ground, MD.

[44] Matney M, How to Calculate the Average Cross-Sectional Area, The Orbital Debris Quarterly News, 2004; 8(2): 7.

[45] Slepian Z, The Average Projected Area Theorem – Generalization to Higher Dimensions arXiv:1109.0595v4 [math.DG] 11 Nov 2012.

[46] Gilbert SM, A model for the effects of condensed phase explosion in a built-up area, Doctoral Thesis, Loughborough University, 1994.

[47] Baker WE, Impact Effects of Industrial Missiles, ASME/PVPD Symposia Volume on Impact, Fragmentation, Blast; Vessels and Piping Systems, S.J. Brown, Editor, 1984(a).

[48] Baker WE, Impact Effects of Industrial Missiles, Impact, Fragmentation, and Blast (Vessels, Pipes, Tubes, Equipment), PVPD/ASME/OAC, S.J. Brown, Editor, 1984(b).

[49] Zaker TA, Fragment and Debris Hazards, AD-A013 634, DDESB TP 12, July 1975, Department of Defense Explosives Safety Board, Washington D.C.

[50] Clemedson CJ, Hellström G, Lindgren S, The relative tolerance of the head, thorax, and abdomen to blunt trauma, Ann. N.Y. Acad. Sci., October 1968; 152(1): 187-198

[51] White CS, The Scope of Blast and Shock Biology and Problem Areas in Relating Physical and Biological Parameters. Technical Progress Report, DASA-1856, Defense Atomic Support Agency, Department of Defense, Washington, D. C., November 1966. Subsequently published in Ann. N. Y. Acad. Sci., 1968; 152(1): 89-102.

[52] Richmond D R, Fletcher ER, Blast Displacement of Dummies on the Surface, Project LN401, Event Dial Pack, Final Report, Lovelace Foundation for Medical Education and Research, Event Dial Pack Preliminary Report, Vol. I-Part II, Defense Atomic Support Agency Information and Analysis Center, Santa Barbara, CA May 1971.

[53] Fletcher ER, Richmond DR, Jonas RK,Blast Displacement of Prone Dummies, Final Technical Progress Report, DASA-2710, Operation Prairie Flat, Project LN-402, Lovelace Foundation for Medical Education and Research, prepared for Defense Nuclear Agency, Washington, DC, 1 June 1971.

[54] Hadjipavlou S, Carr-Hill G, A review of the Blast Casualty Rules Applicable to UK Houses, Home Office Scientific Research and Development Branch, London 1986.

[55] Jones RK, Richmond DR, Fletcher ER, A Reappraisal of Man's Tolerance to Indirect (Tertiary) Blast Injuries, Progress Report, Lovelace Foundation for Medical Education and Research, prepared for Defense Atomic Support Agency, in Proc. Panel N5, Technical Cooperation Program Working Group on Therapy Regimes Meeting, London, April 1969.

[56] Teland JA, Review of blast injury prediction models, Norwegian Defence Research Establishment (FFI) 14 March 2012, FFI-rapport 2012/00539.

[57] Axelsson H, Yelverton JT, Chest Wall Velocity Predictor of Nonauditory Blast Injury in a Complex Wave Environment, J Trauma, 1996; 40(3 Suppl): S31-37.

[58] Li E, Yoshinaka A, Josey T, Weathervane: a single point model for blast injury approximations, 20th Symposium on Military Aspects of Blast and Shock, 2008, Oslo, Norway.

[59] van Doormaal J C A M, van der Horst M J, An approximation of the Axelsson model for quick injury predictions, 21th Symposium on Military Aspects of Blast and Shock, 2010, Jerusalem, Israel.

List of figures

Liste of tables

Annex A   Models for fragment mass and velocity

The fragmentation characteristics below refer mainly to conventional weapons/munitions and are described in several military manuals, such as [A1], [A2], [A3]. These munitions contain some type of high-order explosive charge encased in a metallic container. As explained in these manuals, when the explosive is detonated, the container ruptures into a large number of fragments (of uniform or of different sizes), which are accelerated by the expanding detonation gas products to velocities up to several kilometres per second. It is also stressed that, regarding a specific munition, fragment mass distributions, velocity distributions etc. are best determined by actual arena testing. In the absence of such test data, the methods described below for calculating the casing fragmentation are suggested. Depending on the design of the munition, fragmentation can be: (a) controlled, with the produced fragments retaining their predesigned shape and size, or (b) natural, where the produced fragments will have a wide distribution of size, shape and velocity.

It is expected that several of these methods and relationships can be transferred mutatis-mutandis in the civil security sector, where they can be useful in assessing and countering detonation effects of IEDs with pipe bombs, bombs containing nails and nuts, wire wrappings, etc.

A1.   Fragment mass distribution

The equations below are valid for munitions with cylindrical casing, Figure A1, or one modelled by a series of cylinders, and fragmenting naturally. Among the various formulations and empirical expressions [A-4], [A-5], the fragment mass distribution can be described by the Mott equation

$$\frac{n_f}{N} = \exp\left(-\sqrt{\frac{2m_f}{\overline{m}_f}}\right) \qquad \text{or} \qquad \frac{n_f}{N} = \exp\left(-\frac{\sqrt{m_f}}{M_A}\right) \tag{A1}$$

where, m_f = fragment mass (kg), n_f = expected number of fragments with mass greater than m_f, N = total number of fragments and $\overline{m}_f$ = expected average fragment mass, which depends on the casing and the explosive and is given by the empirical expression

$$\overline{m}_f = 2M_A^2 \tag{A2}$$

M_A is the fragment distribution parameter (with units $kg^{0.5}$) calculated by the formula

$$M_A = B t_c^{5/6} (d_0 - 2t_c)^{1/3} \left(1 + \frac{t_c}{d_0 - 2t_c}\right) \tag{A3}$$

where, B = explosive constant ($kg^{1/2}/m^{7/6}$), d_0 = outside diameter of the munition (m), t_c = thickness of the casing (m). Values for the constant B, which depend on the types of casing and explosive, can be found tabulated in several manuals [A-3], and even though they have been determined empirically for mild steel and cylindrical casing geometry, due to data scarcity, the liberty is taken to use them with other casing materials and configurations.

If M_c is the total mass of the casing, the total number of fragments N is given as

$$N = \frac{M_c}{\overline{m}_f} = \frac{M_c}{2M_A^2} \tag{A4}$$
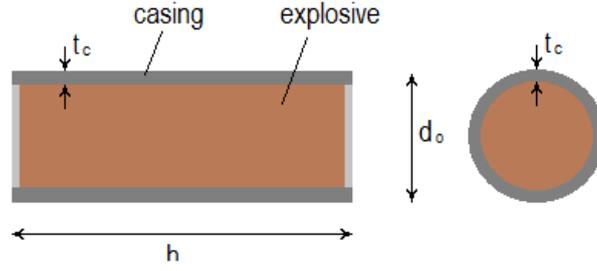
Figure A1. Cylindrical geometry of munition with casing filled with explosive.

Some interesting properties, directly derivable from the Mott equation, can be noticed:

- setting n_f=1, one can find the expected largest mass fragment: $m_{f,max} = M_A^2 (lnN)^2$

- setting m_f=0 gives n_f=N, i.e. the total number of fragments.

It is also observed that the Cumulative Distribution Function $F(m_f)$ and the Probability Density Function $f(m_f)$ for the fragment mass mf can be determined, respectively, as follows

$$F(m_f) = 1 - \frac{n_f}{N} = 1 - \exp\left(-\frac{\sqrt{m_f}}{M_A}\right) \tag{A5}$$

$$f(m_f) = \frac{dF(m_f)}{dm_f} = \frac{1}{2M_A\sqrt{m_f}} \exp\left(-\frac{\sqrt{m_f}}{M_A}\right), \qquad m_f > 0 \tag{A6}$$

It can be checked that $\int_0^\infty f(m_f)dm_f = 1$, as it should, and that the mean value of m_f is $\int_0^\infty m_f f(m_f)\, dm_f = 2M_A^2$, as expected according to eq.(A2).

For completing the setting of the Mott equation, the volume V_c and the total mass M_c of the casing are also expressed, respectively, by the equations

$$V_c = \pi(d_0 t_c - t_c^2)h \quad \text{and} \quad M_c = V_c \rho_c \tag{A7}$$

where, the newly introduced symbols stand for h = height of the cylinder (m) and ρ_c = density of the casing (kg/m3).

A2. Initial Velocity

In the absence of more accurate calculations (with FEM techniques etc.), the initial velocity of the fragments of a munition can be provided by the Gurney equation [A-6]

$$V_o = \frac{G}{\left(\dfrac{M_c}{M_e} + \dfrac{n_g}{n_g + 2}\right)^{0.5}} \tag{A8}$$

where, V_o = initial fragment velocity (m/s), G = Gurney characteristic velocity (m/s), M_c = mass of the casing (kg), M_e = mass of the explosive (kg), n_g = 1 for plane geometry, n_g = 2 for cylindrical geometry, and n_g = 3 for spherical geometry, Table A1. A uniform thickness of the casing is considered along with several other assumptions, whereas instructions are included for more complicated geometries [A-6]]. The values for the

Gurney characteristic velocity G can also be found tabulated in several manuals [A-3], and they have been determined experimentally, mainly for mild steel casings. Approximate formulae for its calculation are also provided there for explosives for which the G is not known, as well as proposals for its more accurate determination.

Table A1. Values of the n_g parameter of the Gurney formula.

Section Type	n_g	Section Geometry
Planar	$n_g = 1$	$\dfrac{M_c}{2}$ $\dfrac{M_c}{2}$ M_e
Cylindrical	$n_g = 2$	M_c M_e
Spherical	$n_g = 3$	M_c M_e
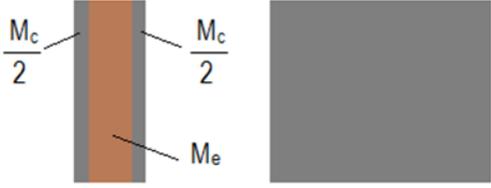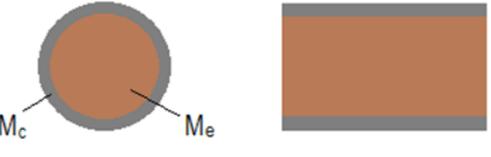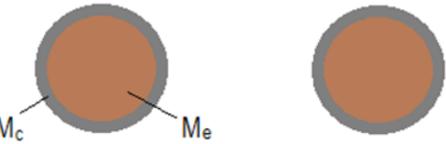
With regards to the reliability of the Gurney formula predictions, as mentioned in the manuals [A-3]

- for munitions with elongated, cylindrical-symmetric shape the fragment velocities calculated with the Gurney formula approximate well those at the munition midsection (whose values may be double the velocity values of fragments at the munition ends);

- the Gurney formula is more suitable for smaller fragments (less than a few grams) and it may over-predict the velocity of larger fragments;

- interestingly, the Gurney velocity predictions are independent from the fragment mass and shape.

Reported typical initial fragment velocity values are between 1200 and 2000m/s.

A3. Variation of fragment velocity with distance

Air drag and gravity affect the motion of a flying fragment reducing its initial velocity V_o. If a constant drag coefficient is assumed and gravity is disregarded in the equations of motion, the fragment velocity, as a function of distance, can be estimated based on the formulae [A-3], [49]

$$V_R = V_o \exp\left(-\frac{R}{L}\right) \qquad \text{with} \qquad L = \frac{2\,k^{2/3} m_f^{1/3}}{C_d\,\rho_a} \tag{A9}$$

where, V_R = velocity at distance R (m/s), V_o = fragment initial velocity (m/s), R = distance from the detonation center (m) of point under consideration, m_f = fragment mass (kg), C_d = drag coefficient, ρ_a = density of air (kg/m³), k = fragment shape factor or "ballistic density" (kg/m³), already introduced in Section 6.4, $k = m_f / A^{3/2}$ with A being the fragment presented area. Clearly, the parameter L represents the distance in which the fragment velocity drops to 1/e of its initial value.

Two distance ranges and launching modes are next distinguished and two conservative equations are correspondingly proposed for the estimation:

- near-field (low angles of fragment departure)

$$V_R = V_o \exp\left(- \frac{1}{2} \frac{C_d \rho_a}{k^{2/3} m_f^{1/3}} R\right)$$ (A10)

- far-field (large angles of fragment departure)

$$V_R = \sqrt{gL} = \sqrt{g \frac{2 k^{2/3} m_f^{1/3}}{C_d \rho_a}}$$ (A11)

The latter expression gives a constant value physically representing the terminal fragment velocity in free fall; g= 9.81 m/s^2 is the gravity acceleration. Finally, according to reference [tripartite], when the distance R is less than 6m, the variation of fragment velocity may be neglected.

The average drag coefficient values over the range of expected fragment velocities is presented in Table A2 for four typical idealised fragment shapes.

Table A2. Average values for drag coefficient C_d

Fragment Shape	Average C_d
Long Rectangular Parallelepipeds and Random Shell Fragments	1.24
Spheres	0.95
Cubes and Cylinders of L/d=1	1.13
Notched Wire of L/d=3	1.20

L = length, d = diameter

A4. A simple example case

A munition is considered having an outer diameter of 0.35m, a height of 0.90m, and a casing thickness of 0.02 m made of steel. The shape of the casing is cylindrical and it is filled with RDX. Given: explosive density ρ_e =1770kg/m^3, explosive constant B= 2.595 kg$^{0.5}$/m$^{7/6}$, Gurney characteristic velocity G= 2925m/s, casing steel density ρ_c =7800kg/m^3, air density ρ_a =1.225kg/m^3.

The application of the above equations for fragmentation concerning fragment distribution and velocity is shown below:

- Volume of casing (no base caps are considered): V_c = π(0.35x0.02-0.02^2)0.90 = 0.0187 m^3
- Total mass of casing: M_c= 0.0187x7800 = 145.56 kg
- Fragment distribution parameter: M_A=2.595x0.025/6(0.35-2x0.02)1/3(1+0.02/(0.35-2x0.02))= 0.07177 kg$^{0.5}$
- Total mass of explosive: M_e= {π(0.35-2x0.02)2/4}x0.90x1770 = 120.23 kg
- Mean mass of fragments: $\bar{m}_f$ = 2x0.071772 = 0.0103 kg
- Total number of fragments: N = 145.56/0.0103 = 14132

- Largest mass fragment: $m_{f,max}$ = 0.071772(ln14132)2 = 0.4704 kg
- Mott equation: $n_f = 14132 \exp(-\frac{\sqrt{m_f}}{0.07177})$

Thus, the number of fragments with mass greater than $\bar{m}_f$ =0.0103kg is $n_f\approx$3436 (and of those with less than $\bar{m}_f$ is 10696= 14132-3436). The number of fragments with mass greater than m_f = 0.050kg is $n_f\approx$627 and of those with less than that is 13505, see Figure A2. The PDF and CDF of the fragment mass are also plotted in Figure A3.
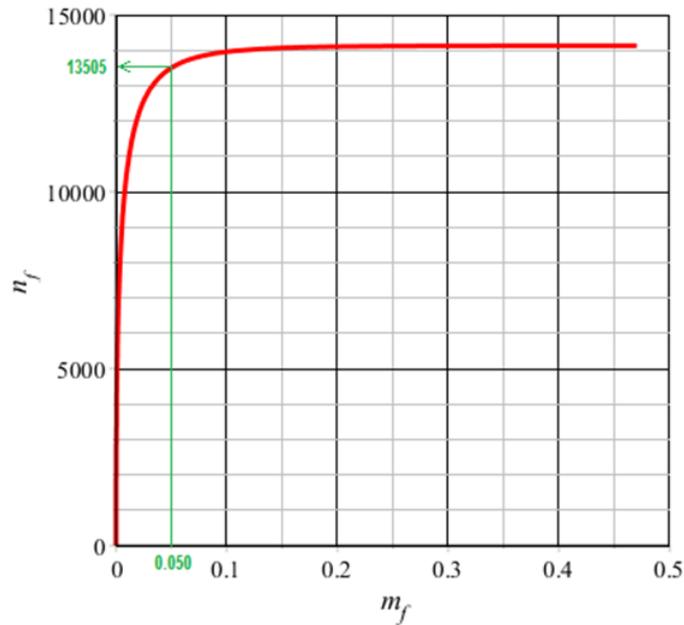

Figure A2. Plot of the Mott equation for the example case.
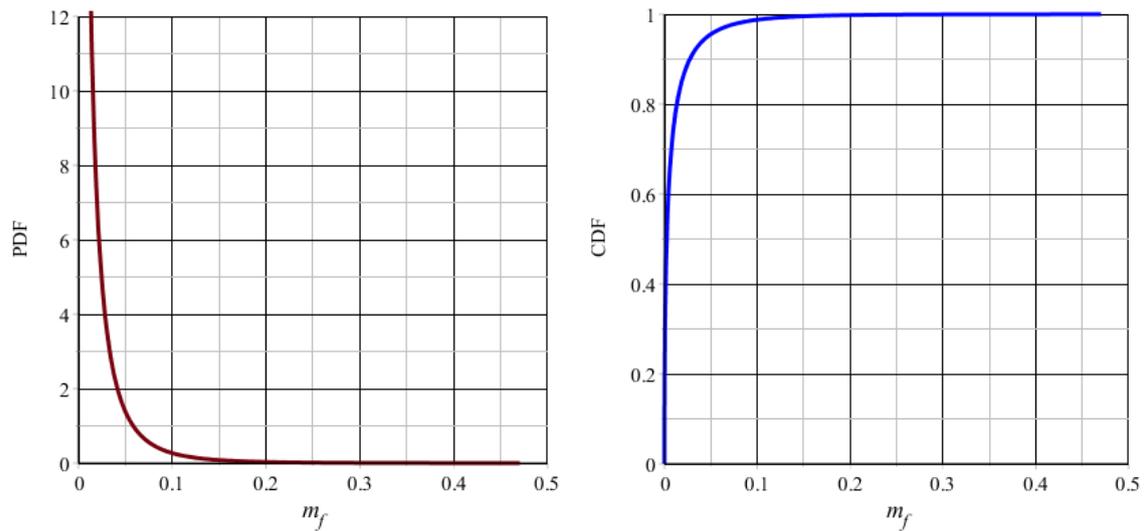
Figure A3. Plot of the PDF and CDF of the fragment mass for the example case.

- Initial velocity of fragments using n_g=2 : V_o = 2925/[145.56/120.23 + 2/(2+2)]$^{0.5}$ = 2236.4 m/s
- Fragment velocity variation with distance:

i) Assuming that some fragments have a cubic or cylindrical shape, the parameter values selected are C_d=1.13 and k=4246kg/m³ (see Section 6.4). The curves showing the variation of the fragment velocity with distance are plotted in Figure A4.a for three fragments having, correspondingly, masses: $10\,\bar{m}_f$, $\bar{m}_f$ and $0.1\,\bar{m}_f$. It is observed that the velocity decrease of lighter fragments is stronger than that of the heavier ones. For the same three masses the far-field velocities (for large launching angles), which represent free-fall conditions, are estimated to: 41.81 m/s, 28.50 m/s and 19.42 m/s, respectively, which indicate that heavier mass fragments reach larger terminal velocity values.

(a)   (b)
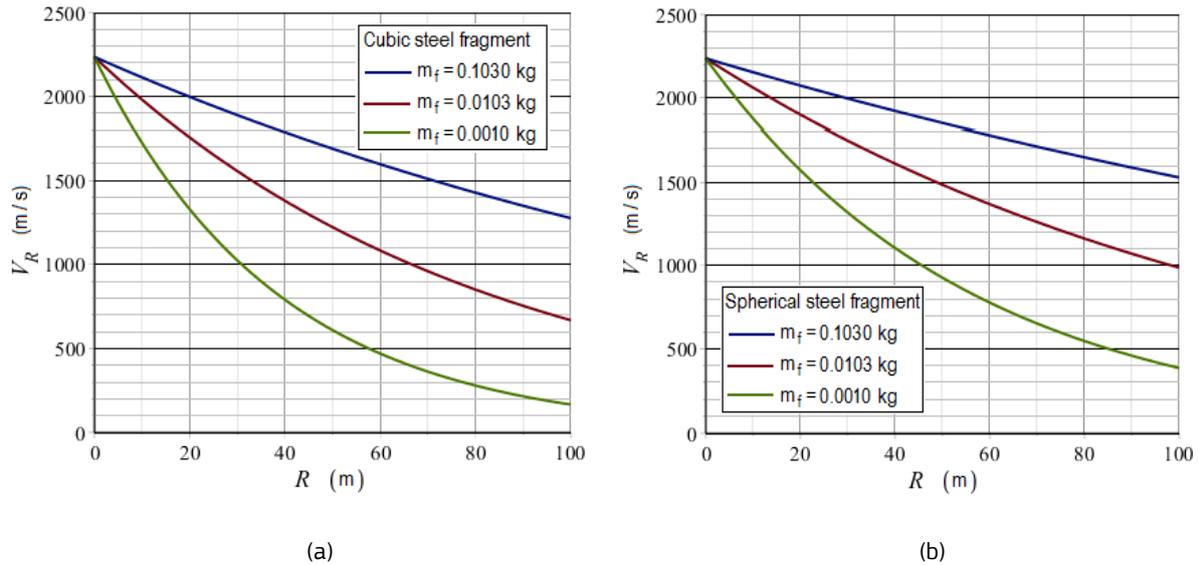
Figure A4. Fragment velocity variation with distance for low launching angles, (a) cubic steel fragments, and (b) spherical steel fragments.

ii) Assuming spherical geometry for the above three fragments, for which C_d=0.95 and k=5867kg/m³ (see Section 6.4), the velocity decay curves are plotted in Figure A4.b, where again it is observed that lighter fragments slow down faster. The far-field velocities (for large launching angles and free-fall conditions) are estimated to: 50.80 m/s, 34.62 m/s and 23.60 m/s, respectively.

As expected, these graphs demonstrate that spherical fragments are overall damped less than the cubic ones. It is finally recalled that the above calculations and results are more representative and realistic for smaller fragments originating from the midsection of the cylindrical munition.

References

[A-1] U.S. Department of the Army, Structures to Resist the Effects of Accidental Explosions, Technical Manual TM 5-1300, November 1990.

[A-2] U.S. Department of the Unified Facilities Criteria (2008), "UFC 3-340-02 Structures to Resist the Effects of Accidental Explosions", U.S. Army Corps of Engineers, Naval Facilities Engineering Command, Air Force Civil Engineer Support Agency

[A-3] Manual of NATO Safety Principles for the Storage of Military Ammunition and Explosives, STANAG AASTP-1, May 2010

[A-4] Elek P, Jaramaz S, Size distribution of fragments generated by detonation of fragmenting warheads, 23rd International Symposium on Ballistics, Tarragona, Spain, 2007.

[A-5] Mott NF, Fragmentation of Shell Cases, Proceedings of the Royal Society of London, Series A (Mathematical and Physical Sciences), 1947; 189: 300-308.

[A-6] Gurney RW, The Initial Velocities of Fragments from Bombs, Shells and Grenades, Report BRL 405, 1943, Army Ballistic Research Laboratories, Aberdeen Proving Ground, MD, USA.

The European Commission's science and knowledge service
Joint Research Centre

JRC Mission
As the science and knowledge service of the European Commission, the Joint Research Centre's mission is to support EU policies with independent evidence throughout the whole policy cycle.

EU Science Hub
ec.europa.eu/jrc

@EU_ScienceHub

EU Science Hub – Joint Research Centre

EU Science, Research and Innovation

EU Science Hub

Publications Office
of the European Union